University of Alberta

Mapping and characterization of *mel-43(sb41)*, a gene required for early embryonic viability in *C. elegans*

by

Donna Curtis Pahara

A thesis submitted to the Faculty of Graduate Studies and Research
in partial fulfillment of the requirements for the degree of

Master of Science

in

Molecular Biology and Genetics

Department of Biological Sciences

Spring 2010
Edmonton, Alberta

Examining Committee

Martin Srayko, Department of Biological Sciences

Frank Nargang, Department of Biological Sciences

Nicolas Touret, Department of Biochemistry

Abstract

A genetic screen for dominant, temperature-sensitive, maternal-effect embryonic lethal mutations identified *mel-43(sb41)*, a gene required for early embryonic viability (Mitenko *et al.,* 1997). Linkage mapping placed *mel-43* within a small region on chromosome IV. Genetic analyses suggested that *mel-43(sb41)* was a neomorphic mutation. While refining the genetic position of the *mel-43* gene, data suggested that the genetic position of *mel-43* was inconsistent with the published location. In light of this new location, previous conclusions regarding the genetic behaviour of *mel-43(sb41)* were re-examined. Deficiency analysis suggests that *mel-43(sb41)* is a haplo-insufficient loss-of-function mutation. *mel-43(sb41)* embryos are significantly delayed in meiosis II independent of cyclin B1 degradation. Consequently, embryos fail to produce meiosis II polar bodies and do not establish proper polarity. Although the function of *mel-43* remains unknown, the persistent meiotic spindle suggests that *mel-43* acts upstream of the microtubule rearrangements necessary to promote the metaphase II to anaphase II transition.

Acknowledgements

There are numerous individuals that I would like to thank who have directly or indirectly contributed to this thesis. I would especially like to thank Marty for welcoming me into his laboratory and for providing direction and insight into my project. Thank you for your support both in the lab and out. The past two and a half years have been an experience that will stay with me forever. To my labmates – Eva, Cheryl, Karen, and Jen - you were an invaluable source of relief from everyday problems and mapping frustrations, and I will always cherish the hilarious moments that we experienced together. *Viva la Sea elegans*!

Thank you to my friends and family for always believing me and for always pushing me to go further with my studies. To my husband, Justin, your accomplishments and ambition are a continued source of inspiration and your belief in me is what made this thesis possible. To Mom, Dad, Katy and David -this wouldn't have happened without your love and support. Thank you to my amazing friends for always being encouraging. I've been fortunate to have you in my life, and look forward to the next adventure.

Table of Contents

List of Tables

List of Figures

List of Symbols, Abbreviations and Nomenclature

°C	Degrees Celsius
AB	Anterior daughter cell
AP	Anterior-posterior
APC/C	Anaphase promoting complex/cyclosome
ATP	Adenosine triphosphate
BLI	Blistered
Bp	Base pair
CDK	Cyclin-dependent kinase
CKI	Cyclin-dependent kinase inhibitor
CUL	Cullin
CYB	Cyclin B
DIC	Differential interference contrast
DNA	Deoxyribonucleic acid
DPY	Dumpy
DTC	Distal tip cell
ELC	Elongin C
FEM	Feminization of XX and XO animals
GFP	Green fluorescent protein
γTuRC	γ-tubulin ring complex
GTP	Guanosine triphosphate
HECT	Homologous to the E6-AP carboxyl terminus
KLP	Kinesin-like protein
MAT	Metaphase-to-anaphase transition defective
MAPK	Mitogen-activated protein kinase
MEL	Maternal effect embryonic lethal
mRNA	Messenger ribonucleic acid
MSP	Major sperm protein
NEBD	Nuclear envelope breakdown
NGM	Nematode growth medium
P1	Posterior daughter cell
PAR	Partitioning defective
PB	Polar body
PBS	Phosphate buffered saline
PCM	Pericentriolar material
PCR	Polymerase chain reaction
RanGTP	Ras-related nuclear protein bound to GTP
RBX	Ring-box
RE	Restriction enzyme
REC	Abnormal Recombination
RING	Really interesting new gene
RNA	Ribonucleic acid

RNAi	Ribonucleic acid interference
ROL	Roller
SNP	Single nucleotide polymorphism
SP	Spermatheca
U Box	Ubiquitination box
UNC	Uncoordinated
UT	Uterus
VU	Vulva
WT	Wild-type
ZYG	Zygote defective

1. Introduction

1.1. Introduction to *Caenorhabditis elegans* and its germline

In the past four decades, *Caenorhabditis elegans* has been established as an excellent model organism for the study of eukaryotic genetics and cell biology. Genetics is simplified in this self-fertilizing hermaphroditic nematode because homozygous recessive phenotypes can be analyzed without tedious test-crossing. However, males also exist and can be used as a vehicle to transfer mutations across strains. Of particular interest to this thesis is the early embryo of the worm, which is ideal for studying the dynamic cell biology of a single cell. In addition, a multitude of techniques have been developed and/or refined in *C. elegans* including: genetic screens, RNA interference (RNAi), light and fluorescence microscopy, and transformation by microinjection or microparticle bombardment.

At 20°C *C. elegans* requires approximately three days to progress from a newly laid egg to an egg-laying hermaphrodite. This is a temperature-dependent cycle and worms are routinely maintained at 15°C, 20°C, or 25°C, depending on the desired rate of development. Though *C. elegans* populations are primarily hermaphroditic, a successful mating between male and hermaphrodite results in approximately 50% males in the subsequent generation. Although most analyses are carried out in the hermaphrodite, or

the eggs thereof, males prove to be very useful for crossing genetic markers into and out of various strains, and for creating new heterozygous strains.

The reproductive machinery of the L4/young adult hermaphrodite is quite streamlined (Figure 1-1). Two reflexed gonad arms (with a distal–proximal axis), each containing a syncitium of germline nuclei, are visible using differential interference contrast (DIC) optics. As the nuclei progress into the proximal gonad arm, they mature into oocytes. The most proximal region of each gonad arm is continuous with a spermatheca compartment, which houses mature sperm. The two spermathecae open into a single uterus, where young embryos undergo early cleavages before being expelled through the vulval orifice.

Mitotic germline nuclei are continually produced at the distal end of the gonad, controlled by signaling from the distal tip cell (DTC; Kimble and White, 1981). The cell membranes do not fully enclose these mitotic nuclei, generating the characteristic syncitial gonad in the distal region. In hermaphrodites, the earliest nuclei produced develop into sperm (completed by the 4th larval stage), whereas in the adult the nuclei develop into oocytes. As the gonad nuclei progress proximally along the distal-proximal axis, progressive oocyte maturation occurs. Nuclei enter meiotic prophase after they reach a critical distance from the DTC, a region referred to as the transition zone. Meiotic cells progress partially through meiosis I but arrest in pachytene. Following exit from pachytene, meiosis continues through

diplotene where the chromosomes condense and then progress into diakinesis, where the oocytes arrest for a second time. Conversely, nuclei destined to become sperm exit pachytene and progress through gametogenesis immediately. In both cases, exit from pachytene is dependent on activation of the mitogen-activated protein kinase (MAPK) pathway (Church *et al.,* 1995).

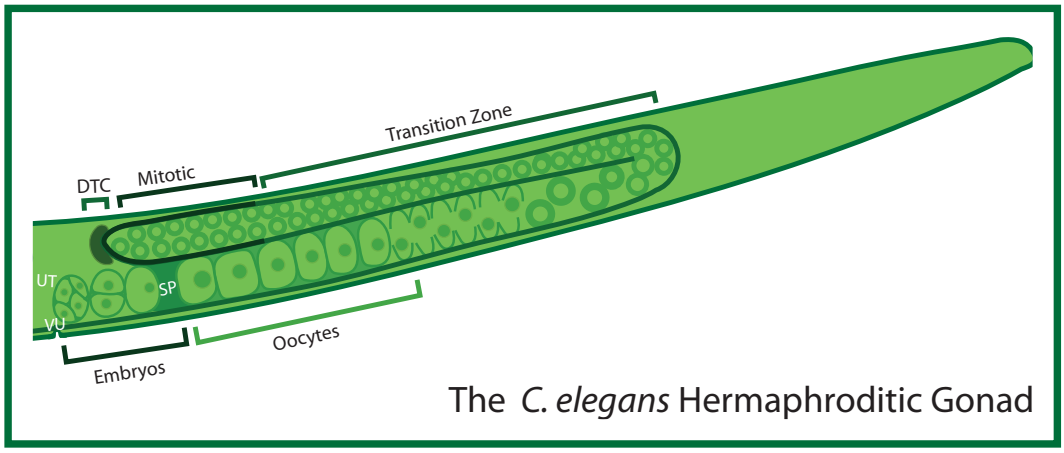

Figure 1-1. The hermaphroditic *C. elegans* gonad. Signaling from the distal tip cell (DTC) produces a syncitium of mitotic germline nuclei in each gonad arm of the hermaphrodite (only one gonad arm is shown). Once the nuclei enter the transition zone they enter meiosis. MAPK and major sperm protein (MSP) signaling govern the progressive maturation of distal nuclei into proximal oocytes. Oocytes are fertilized when they pass through the spermatheca (SP). Embryos undergo early cleavage events in the uterus (UT) and are then expelled through the

In diakinesis, the oocytes undergo vast morphological changes, including accumulation of cytoplasmic and nuclear volume. Oocytes remain arrested in diakinesis until a signal is received from major sperm protein (MSP; Miller *et al.,*

2001). The MSP signal stimulates maturation, sheath cell contraction, and activation of MAPK, which releases the oocyte from the meiotic arrest (Miller *et al.,* 2001). Coupling the sperm MSP signal to oocyte maturation allows for the conservation of cytoplasmic resources; energy is invested in creating an oocyte only if there is a sperm available to fertilize it. In concert with oocyte maturation, cortical rearrangement and nuclear envelope breakdown (NEBD) occurs. This is followed by the accumulation (or appearance) of microtubules in the nuclear region. Sheath cell contraction, modulated by the oocyte, causes the dilation of the spermatheca opening and the sheath cells pull the spermatheca over the oocyte, forcing fertilization to occur (McCarter *et al.,*1999).

1.2. Post-fertilization events in the embryo

1.2.1. Meiosis

Although the oocyte spends about seven minutes in the spermatheca, it is thought that fertilization occurs immediately upon entry (Samuel *et al.,* 2001). Fertilization triggers the assembly of a chitinous eggshell around the developing zygote, which provides physical and osmotic protection for the developing embryo. Sperm entry also initiates polarization of the embryo. The point of sperm entry dictates the posterior pole of the embryo and triggers a cascade of subsequent polarization events, including the

distribution of PAR (partitioning defective) proteins. By the time the oocyte exits the spermatheca and enters the uterus, the first meiotic spindle has usually formed (Yang *et al.,* 2003).

Immediately after fertilization, the *C. elegans* oocyte nucleus harbors four copies of each chromosome. Two successive meiotic divisions are necessary to form a haploid female pronucleus that will then combine with the haploid sperm pronucleus to reconstitute a diploid cell (Figure 1-2). The first meiosis, initiated prior to cellularization of the oocyte, completes shortly after fertilization. The meiotic spindle is oriented in close proximity and perpendicularly to the presumptive anterior cortex. Translocation of the meiotic spindle to the cortex is a microtubule-dependent process (Yang *et al.,* 2003). Bivalents, comprising paired homologous chromosomes with their sister chromatids oriented end-to-end, situate axially (perpendicular to the spindle equator) (Albertson and Thomson, 1993). At anaphase I, homologous chromosomes segregate to each pole. REC-8, a cohesion protein, is partially removed from sister chromatids at this point (Pasierbek *et al.,* 2001), however the chromatids remain closely associated throughout meiosis I. After anaphase has completed, the chromosomes nearest the cortex are extruded out of the cell and packaged into a polar body, which is largely devoid of cytoplasm. This first meiotic division is considered reductional because the genetic information is halved in the process.

The second meiotic spindle assembles immediately after the first polar body extrusion. The second spindle is morphologically similar to the first meiotic spindle and also aligns at the cortex. Sister chromatids assemble end-to-end and orient axially within the spindle. At anaphase II, REC-8 is completely removed from sister chromatids, allowing them to separate, and a haploid complement is extruded as a second polar body (Pasierbek *et al.,* 2001). This final meiosis guarantees that upon pronuclear fusion, the zygote will be diploid.

Each meiotic anaphase concludes with an extremely asymmetric division. In this way, the excess nuclear material (containing two copies of one set of chromosomes in meiosis I, and one copy of the remaining set in meiosis II) is extruded out of the cell in the form of a polar body. It is thought that the small size of the spindle and the close association with the cortex is necessary to ensure that minimal cytoplasm is lost during this process (Yang *et al.,* 2003).

1.2.2. Mitosis

The sperm supplies a haploid pronucleus and also introduces a pair of centrioles to the acentrosomal oocyte. Structurally, the centriole is composed of nine singlet microtubules arranged in a tube; two centrioles orient orthogonally to form a pair. Upon sperm entry, centrioles begin to mature into centrosomes by recruiting pericentriolar material (PCM), which includes

proteins necessary for centrosome duplication and microtubule nucleation. Despite the presence of centrioles in the early meiotic cytoplasm, it is only after meiosis has completed that centrosomes are observed to nucleate microtubules. This regulatory requirement is essential to the integrity of the meiotic spindle; the presence of centrosome-based microtubules could physically interfere with the meiotic spindle, causing chromosome segregation defects.

Following the completion of meiosis, the chromosomes begin to condense and both pronuclei increase in size. The two sperm-derived centrioles split from each other to form two centrosomes, each containing a single centriole that must be duplicated to regenerate a pair. The two centrosomes associate tightly with the sperm-derived pronucleus, and migrate to opposite sides of the pronuclear envelope as they separate. Subsequently, the oocyte pronucleus begins a slow posterior migration towards the sperm pronucleus. This is driven by cytoplasmic flows caused by polarity-induced cortical contractions of the embryo. When centrosomal microtubules make contact with the oocyte pronucleus, they facilitate a faster migration toward the sperm pronucleus. Upon meeting, the two pronuclei and the centrosomal pair relocate to the centre of the embryo and rotate such that the centrosomes are aligned along the long axis of the embryo.

NEBD permits the fusion of the pronuclei, and thus allows the chromosomes to pair and align along the metaphase plate during mitosis.

During metaphase and anaphase the spindle oscillates and is gradually displaced towards the posterior pole. At anaphase this results in an asymmetric cleavage that produces a larger anterior daughter cell (AB) and a smaller posterior daughter cell (P1). The off-set position of the mitotic spindle in the embryo is dependent on proper PAR protein localization (Wu and Rose, 2007). Polarization–induced asymmetry allows the embryo to attribute unique developmental potential to daughter cells by segregation of cell-fate determinants. For example, the smaller posterior P1 cell contains all of the germline components and germ cell proteins are continually segregated to the posterior daughter cell. This eventually results in a posterior-most founder cell that is responsible for the entire germline formation.

1.2.3. Maternal contributions

Upon fertilization, the small amoeboid sperm contributes a pair of centrioles and a haploid genetic complement to the oocyte cytoplasm. Additionally, transcription in the oocyte is silenced from diakinesis onwards and does not reinitiate until the four-cell stage of the early embryo (Reviewed in Blackwell and Walker, 2008). This means that the oocyte, as well as the early embryo, is completely dependent on oocyte proteins and maternally-provided mRNAs for cellular functions. Therefore, the embryo must strictly regulate the translation of certain mRNAs at the proper time in development.

Additionally, degradation of specific RNAs and proteins is necessary for the progression of embryonic development.

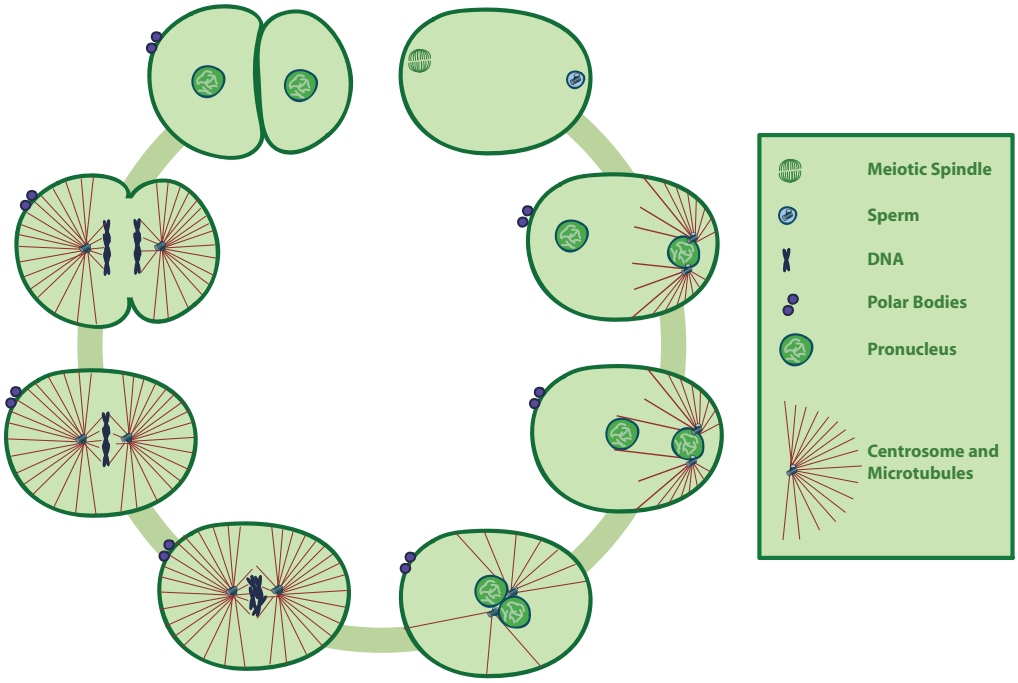

Figure 1-2. Landmark cytoskeletal events in the single cell embryo. Clockwise from top right: Sperm entry triggers the resumption of meiosis, and the extrusion of two polar bodies. After meiosis completes, centrosomes on the sperm-derived pronuclear envelope nucleate microtubules. The female pronucleus begins a slow posterior migration, and this is quickened when centrosomal microtubules make contact with the pronucleus. The two pronuclei meet, centre, and rotate. Nuclear envelope breakdown permits chromosome congression towards the metaphase plate. In mitotic metaphase and anaphase, the spindle displaces to the posterior cortex. At cytokinesis an asymmetric cleavage occurs, generating a smaller posterior P1 cell and a larger anterior AB cell.

1.3. Spindle structure

1.3.1. Microtubules

Arguably the most important component of a spindle is the microtubule. Microtubules are an integral part of the eukaryotic cytoskeleton and are found in all dividing cells and most differentiated cell types. Structurally, microtubules are composed of α- and β-tubulin heterodimers that arrange end-to-end in linear protofilaments. Generally, 13 protofilaments associate with each other to form a hollow tube with a diameter of approximately 25 nm (Moritz *et al.,* 1995a,b).

Due to the nature of the tubulin subunit association, microtubules are both polar and dynamic. The plus end, with exposed β subunits, is faster growing and more dynamic while the minus end, with exposed α subunits, is more stable. The minus end is usually anchored to the centrosome. Microtubules go through periods of growth (polymerization) and periods of destabilization (catastrophe), regulated by the phosphorylation state of a bound GTP molecule. Individual microtubules are always growing and shrinking, but when considered as a population, they are able to reach a steady state providing they are not limited by the cytoplasmic concentration of free tubulin (Mitchison and Kirschner, 1984). This physical property of microtubules allows for control of polymerization and depolymerization rates, as well as the direction of microtubule outgrowth.

Many proteins are able to influence the activity of microtubules by physically associating with the filament. For example, γ-tubulin with accessory proteins forms a γ-tubulin ring complex (γTuRC) that has a diameter of approximately 25 nm. This structure localizes to the centrosomes and acts as a nucleation scaffold for the minus end of microtubules, promoting microtubule organization (Strome *et al.,* 2001). Motor proteins from the kinesin and dynein motor protein families use ATP hydrolysis to move unidirectionally along the microtubule lattice; this movement is primarily harnessed for cargo transport in the cell. Numerous other types of proteins also associate with microtubules and can act as either stabilizing or destabilizing factors.

1.3.2. Meiotic spindle

As in most metazoans, the *C. elegans* oocyte eliminates centrosomes prior to meiosis, thereby ensuring that upon fertilization a proper bipolar spindle will be formed using only sperm-derived centrosomes. In the case of *C. elegans* this is likely mediated by cyclin-dependent kinase inhibitor-2 (*cki-2)*. In *cki-2* mutants, extra chromosomes and multipolar mitotic spindles result from the presence of oocyte-derived centrosomes (Kim and Roy, 2006). The consequence of centrosome elimination during oogenesis is that female bipolar meiotic spindles must form in their absence. In many systems where

centrosomes are not present, microtubule nucleation and organization is directed by the chromosomes. This is accomplished in part by a RanGTP gradient that forms around chromatin; high concentrations of RanGTP at chromatin result in the release of spindle assembly factors that stabilize microtubules or encourage plus-end growth. In *C. elegans*, depletion of Ran does not affect meiotic spindle formation, suggesting that a different mechanism is responsible for the generation of microtubules when centrosomes are absent. (WormBase; Srayko *et al.,* 2005).

Katanin is a microtubule-associated protein with microtubule-severing ability. It was discovered due to the observation that mitotic *Xenopus* egg extract is able to sever long taxol-stabilized microtubules into shorter fragments (Vale, 1991). In *C. elegans* katanin is necessary to organize microtubules into a meiotic spindle (Srayko *et al.,* 2000). In loss-of-function katanin mutants, microtubules still form around the meiotic chromatin but do not organize into a proper bipolar spindle (Clark-Maguire and Mains, 1994). Counter-intuitively, electron tomography experiments in worms indicate that katanin severing helps to generate microtubule polymers during female meiotic spindle assembly (Srayko *et al.,* 2006). Compared to centrosomes, the chromatin is relatively inefficient at nucleating microtubules, therefore in the acentrosomal meiotic environment, katanin severs a few long microtubules and converts them into smaller fragments that can be incorporated into the spindle. The study of *C. elegans* mutants with hyperactive katanin has led to

the discovery that katanin must be degraded through ubiquitin-mediated proteolysis after oocyte meiosis has completed (Clark-Maguire and Mains, 1994b; Pintard *et al.,* 2003a,b). In hyperactive katanin mutants severe mitotic spindle defects are observed, including a misplaced shortened spindle, chromosome segregation errors, and cytokinesis defects (Clark-Maguire and Mains, 1994b; Pintard *et al.,* 2003a,b). Taken together, these data suggest that in *C. elegans*, katanin is necessary during meiosis to increase the number of microtubules, facilitating the organization of free microtubules into a bipolar spindle (Srayko *et al.,* 2006). Furthermore, the regulation of katanin must be strictly controlled so that mitosis is not disrupted by inappropriate microtubule severing.

1.3.3. Mitotic spindle

The mitotic spindle is morphologically distinct from the meiotic spindle, even though they are formed in a common cytoplasm. The primary structural difference is the presence of centrosomes in mitotic spindles. Centrosomes, containing γ-TuRCs, are proficient microtubule nucleating and organizing centres. This means that mitotic spindles, composed of kinetochore and non-kinetochore microtubules, are generously proportioned and can be positioned within the cell by astral microtubules contacting the cortex.

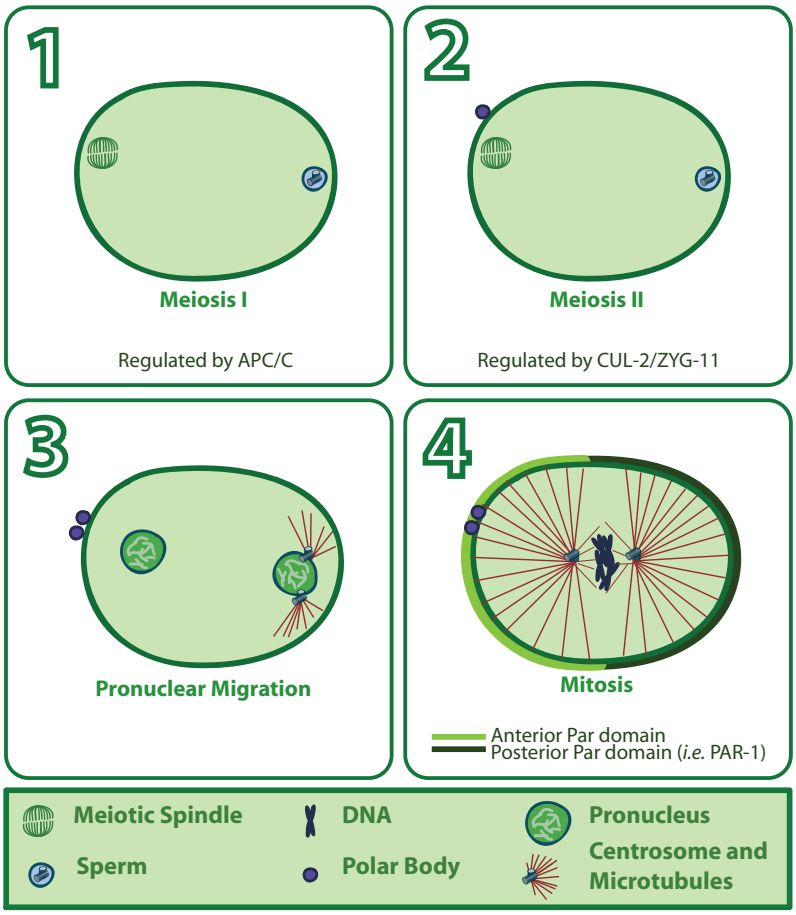

Figure 1-3. Meiotic and mitotic spindles in the one-cell embryo. 1. Sperm entry triggers the resumption of meiosis I. 2. Following the first polar body extrusion, the second meiotic spindle forms and is morphologically similar to the first meiotic spindle. 3. Following the second polar body extrusion in meiosis II, the centrosomes begin nucleating microtubules at the posterior end of the embryo. The DNA condenses and pronuclei are observed in the cytoplasm. 4. After pronuclear meeting, the one-cell mitotic embryo assembles in the middle of the embryo and anterior and posterior Par domains establish. .3

1.4. Meiosis to mitosis transition

1.4.1. Ubiquitin-mediated proteolysis

The progression through meiosis I and II requires the targeted degradation of key proteins that otherwise prevent the progression of cellular processes. Degradation of these key proteins is primarily mediated by ubiquitination of substrates and their destruction via the proteasome. The majority of mutations that result in a meiotic phenotype can be directly tied to this degradation pathway, implicating its importance in meiosis. For instance, an E3 ubiquitin-protein ligase complex is responsible for degradation of katanin at the end of meiosis (Pintard *et al.,* 2003a,b). Although ubiquitin-mediated degradation is essential for many post-embryonic processes in the developing organism, its debut is in meiosis. For example, RNAi depletion of the proteasome components or of ubiquitin itself, results in the arrest of the embryo at the one-cell stage during meiotic divisions (Gönczy *et al.,* 2000; Takahashi *et al.,* 2002).

In *C. elegans* the machinery for this ubiquitin-mediated proteolysis consists of a single 26S proteasome, ubiquitin, one ubiquitin-activating enzyme (E1), over 20 ubiquitin-conjugating enzymes (E2s), and hundreds of ubiquitin-protein ligases (E3s). Protein ligases can be separated into four categories: HECT-domain proteins; U-box proteins; monomeric RING finger proteins; and multimeric complexes that contain a RING finger protein (Reviewed by

Kipreos, 2005). The multimeric RING finger complex class can be further separated into cullin-based complexes and the anaphase promoting complex/cyclosome (APC/C) that contains a cullin-like protein, APC2.

1.4.2. Regulation of meiosis I

The APC/C is well known for its role in initiating the separation of chromatids during anaphase of mitosis, but in yeast and *C. elegans* it is necessary for meiotic divisions as well (Golden *et al.,* 2000; Davis *et al.,* 2002). In the *C. elegans* oocyte, the APC/C is integral to the first meiotic division as it dictates the transition from metaphase I to anaphase I. This is accomplished by the degradation of securin, which releases the cysteine protease separase from inhibition and allows cleavage of cohesions, protein complexes that bind sister chromatids (Davis *et al.,* 2002). Additionally, the degradation of B-type cyclins at this time inactivate cyclin-dependent kinases (CDKs) and promotes exit from metaphase (Liu *et al.,* 2004; Sonneville and Gönczy, 2004). Null mutations in components of the APC/C cause embryos to arrest at the one-cell stage prior to polar body production (Golden *et al.,* 2000). A study of hypomorphic APC/C mutations showed that meiosis II is not as sensitive to mutations in the APC/C and is regulated by an independent pathway (Shakes *et al.,* 2003).

1.4.3. Regulation of meiosis II

Recent work has shown that meiosis II is regulated by a cullin-based E3 ligase complex containing the cullin CUL-2 (Liu *et al.,* 2004; Sonneville and Gönczy, 2004). CUL-2 is a protein ligase that functions in a complex with the adaptor protein elongin C (*elc-1*) and the ring-box 1 protein (*rbx-1*; Liu *et al.,* 2004). A substrate recognition subunit for CUL-2, ZYG-11, binds elongin C to directly interact with the CUL-2 E3 complex (Vasudevan *et al.,* 2006). *cul-2* mutants exhibit no significant defects in meioisis I, however they usually exhibit metaphase II delays and fail to complete anaphase. Mutations in *zyg-11* cause a meiotic delay, but most mutant embryos complete anaphase without extruding a polar body. The cause of the meiosis II delay has been at least partially attributed to the inability of the complex to degrade B-type cyclins: removal of CYB-1 by RNAi in *cul-2* mutants partially rescues the meiotic delay, but is unable to rescue the anaphase defect (Liu *et al.,* 2004).

1.4.4. Transitional requirements

A number of requirements must be satisfied in order for an embryo to begin mitotic spindle assembly. Because the meiotic and mitotic spindles are formed in the same cytoplasm in the absence of zygotic transcription, the proteins that are required for their respective assembly and function must be precisely regulated. Meiotic-specific proteins must be removed or inactivated

so that they do not interfere with the mitotic spindle apparatus. For example, katanin is necessary for meiosis but detrimental if it is still present during mitosis. Likewise, mitosis-specific proteins or structures must be repressed until they are needed; if the mitotic spindle were to assemble prior to the completion of meiosis, it could structurally interfere with the meiotic spindle. Therefore, it is imperative that the initiation of mitosis be temporally coordinated with the completion of meiosis.

1.5. Discovery and identification of *mel-43(sb41)*, a maternal-effect embryonic lethal mutation

mel-43(sb41) was identified in a large scale screen for dominant, temperature-sensitive, maternal-effect embryonic lethal mutations (Mitenko *et al.,* 1997). The screen was designed to identify redundant genes affecting embryonic development. Such genes could be confirmed as nonessential or redundant by determining the null phenotype, as functional redundancy could be more prevalent for genes that are involved in processes requiring a high degree of fidelity. Although complete redundancy between two or more genes is relatively rare, partial redundancy seems to be common in *C. elegans*: if after a gene duplication event the paralogues acquire additional roles, it is likely that they will not be selected against, as their retention provides added protection against the loss of the related gene (reviewed in Cooke *et al.,* 1997).

Using three-factor mapping, *mel-43(sb41)* was placed in the genetic interval between *unc-24* and *fem-3* on chromosome IV (Mitenko *et al.,* 1997). The mutation was complementation tested with known maternal and zygotic lethal genes in the region and determined to be a new mutation.

mel-43(sb41) also satisfied the temperature-sensitive requirement inherent in the screen. Homozygous *mel-43(sb41)* animals were viable but showed little or no hatching at the permissive temperature of 15°C. Using Nomarski microscopy, live homozygous *mel-43(sb41)* embryos displayed abnormally small spindles, synchronous cell division at the two–cell stage and, in many embryos, a failed cytokinesis. Intragenic revertants were found at an appreciable frequency (1/525). Two of these revertants, *sb41sb67* and *sb41sb69* were characterized and used for morph classification. Two deficiencies in the region, *eDf18* and *eDf19* (that together fail to completely delete the region), were also tested *in trans* to the mutation. When homozygous, the revertants had wild-type levels of hatching. Regardless of whether *sb41* was placed *in trans* to either the revertants, wild-type chromosomes, or deficiencies, similar levels of hatching were observed. The high level at which the revertants were recovered suggested to the researchers that they were actually loss-of-function alleles of *mel-43*, and the behaviour of the alleles when homozygous implied that the null phenotype was wild-type. Because the effect of one copy of the *mel-43(sb41)* mutation was unchanged in the presence of a wild-type allele (*mel-43(sb41)*/+), in the

presence of a putative null allele (*mel-43(sb41)/sb41sb67* or *mel-43(sb41)/sb41sb69*), and in the presence of a deletion (*mel-43(sb41)/eDf18* or *mel-43(sb41)/eDf19*), it was concluded that dosage of the wild-type allele is not responsible for the phenotype. These data and interpretations suggested that *mel-43(sb41)* was neomorphic and likely exerts a novel cellular function.

1.6. Goals of this thesis

There were two major aims of this thesis. The first was to identify the *mel-43* gene through a combination of genetic mapping and transformation rescue of the *sb41* mutation. The second was to further characterize *mel-43(sb41)* embryos in order to gain some insight into the molecular basis for the mutant phenotype.

1.7. Summary of this thesis

Although originally reported to map to chromosome IV between *unc-24* and *fem-3*, evidence is presented herein that the *mel-43* locus is located nearly four map units away from this original location, between the *unc*-17 and dpy-*13* loci. In light of this finding, previous genetic characterization of *mel-43(sb41)* and interpretations of the data must be re-examined. The *mel-43*

locus is deleted by the deficiency *mDf9*. The genetic behaviour of *mel-43(sb41) in trans* to *mDf9* suggests that *mel-43(sb41*) is haplo-insufficient.

In addition to providing a new physical location for *mel-43*, this work shows that *mel-43(sb41)* embryos are severely delayed in meiosis II and enter mitosis after failing to produce the second polar body. Because of this, embryos contain extra nuclei that participate in the mitotic division. The meiotic delay appears to be independent of cyclin B degradation. Numerous cytoskeletal and cytokinetic defects are observed in *mel-43(sb41)* embryos. One-cell *mel-43(sb41)* embryos fail to establish proper cortical polarity and consequently fail to divide asymmetrically.

2. Materials and methods

2.1. Nomenclature

C. elegans genes are designated by a three or four letter name that typically describes its mutant phenotype or its molecular nature. The name is followed by a hyphen and an Arabic number, all of which are italicized (i.e. *dpy-20*). Each mutation is given a unique laboratory code of one to three letters, followed by an Arabic number (*i.e. e1282*). When the gene and mutation are used together, the allele is placed in parentheses behind the gene name (*i.e. dpy-20(e1282)*). Protein products of a gene are designated by writing the gene name in uppercase, non-italicized letters (*i.e.* DPY-20). Phenotypes can be described using the complete word (*i.e.* Dumpy) or by using a three or four letter abbreviation, where the first letter is capitalized (*i.e.* Dpy). Strains consist of two or three uppercase letters followed by a number. Each laboratory has a specific strain designation (*i.e.* MAS is specific to the Srayko Laboratory).

2.2. Strains and stock maintenance

All strains of *C. elegans* (var. Bristol) were maintained according to Brenner (1974) at 20 ˚C, unless otherwise indicated. Nematode Growth Medium (NGM) plates were seeded with a uracil auxotrophic *E. coli* strain, OP50. Strains were

obtained from the *Caenorhabditis* Genetics Centre (CGC) with the exception of the following: Strain HR592 was obtained directly from Dr. Paul Mains' laboratory (University of Calgary), strain ET113 was graciously sent by Dr. Edward Kipreos (University of Georgia) and CB138 was obtained from Dr. Dave Pilgrim (University of Alberta). MAS-designated strains were made in the Srayko Laboratory.

Strain	Genotype
HR592	*mel-43(sb41) dpy-20(e1282)/nT1[unc(n754dm) let]* IV*; +/nT1* V
CB138	*unc-24(e138)* IV
BE16	*bli-6(sc16)* IV
CB1893	*unc-17(e113) dpy-13(e184)* IV
SP1052	*dpy-13(e184) unc-5(e53)* IV
ET113	*pie-1::GFP-cyb-1*
DR684	*mDf9/nT1* IV; *+/nT1* V
DR1786	*dpy-13(e184) unc-24(e138)* IV; *mDp4 [unc-17(e245)]* (IV;?)
TH11	*unc-5(e53) dpy-20(e1282)* IV
TH32	*unc-119(ed3) ruIs32* III; *ddIs6*
TH27	*unc-119(ed3)* III; *ddIs6*
AZ244	*unc-119(ed3)* III; *ruIs57[unc-119(+)pie-1::GFP::tubulin]*
MAS87	*mel-43(sb41) dpy-20(e1282)/nT1* IV*; +/nT1* V
MAS88	*mel-43(sb41) dpy-20(e1282)/nT1[unc(n754dm) let]* IV*; +/nT1* V; *pie-1::GFP::tubulin*
MAS89	*mel-43(sb41) dpy-20(e1282)/nT1[unc(n754dm) let]* IV*; +/nT1* V; *pie-1::GFP::cyb-1*
MAS90	*mel-43(sb41) dpy-20(e1282)/nT1[unc(n754dm) let]* IV*; +/nT1* V; *unc-119(ed3) ruIs32* III

Table 2-1. *Caenorhabditis elegans* strains used in this thesis.

mel-43(sb41) was maintained as a balanced heterozygote at 15 ˚C. In HR592, the translocation *nT1[unc(n754dm) let]* contains a linked dominant Unc marker and a recessive lethal, allowing the identification of all progeny.

HR592 was maintained by picking individual Unc worms and checking for proper segregation of parental heterozygotes: Uncs (*mel-43(sb41) dpy-20/nT1[unc(n754dm) let]*, Dpys (*mel-43(sb41) dpy-20* homozygotes) and dead eggs (*nT1[unc(n754dm) let]* homozygotes) are all expected. Transgenic derivatives of HR592 that were constructed were also maintained in a heterozygous balanced state at 15 ˚C.

The following transgenic strains were made: MAS88 β-Tubulin::GFP; *mel-43(sb41)*, MAS90 histone::GFP; *mel-43(sb41)*, and MAS89 *cyb-1*::GFP; *mel-43(sb41)*. A general crossing scheme for incorporation of GFP transgenes into the *mel-43(sb41)*-containing strain is outlined in Figure 2-1. The GFP transgenes are expressed under control of the germline promoter, *pie-1* (Praitis *et al.,* 2001).

2.3. Worm lysis and sequencing

For preparation of genomic DNA for candidate gene sequencing, multiple gravid hermaphrodites were picked into a small volume of Worm Lysis Buffer (50mM KCl, 10mM Tris pH 8.3, 2.5mM $MgCl_2$, 0.45% NP-40, 0.45% Tween-20, 0.01% Gelatin) that had a final concentration of 1mg/mL Proteinase K added. Lysis was achieved by heating the mixture to 65 ˚C for 60 minutes and then inactivating proteinase K by heating to 95 ˚C for 15 minutes. Sequencing was

performed by the Molecular Biology Service Unit (MBSU) at the University of Alberta.

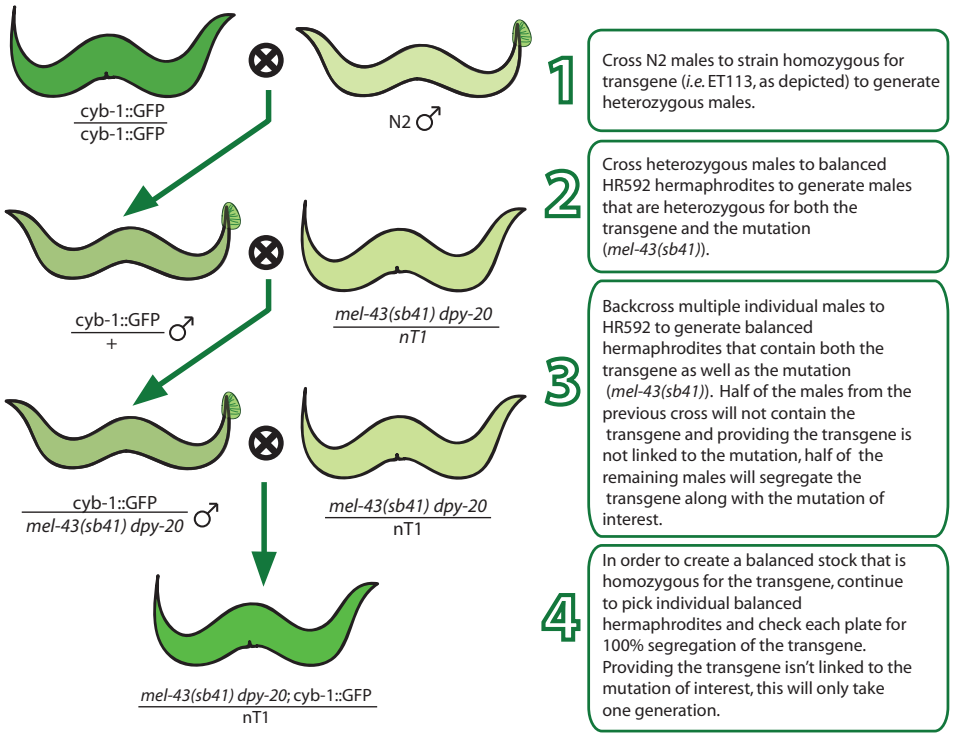

Figure 2-1. General crossing scheme for transgene incorporation.

Primer Name	Primer Sequence	Target
SJJ_C28C12.2_F	5′ - TCG AAT ATT TCT TGC AGA TGC TT -3′	C28C12.2
SJJ_C28C12.2_B	5′ - ATT CCT GTT TGC GTA TGA ACA CT -3′	C28C12.2
C33H5.4_Seq1	5′ - GAA CAC GTT TTC CAG CAT CTG -3′	C33H5.4
C33H5.4_Seq2	5′ - CAG ATG CTG GAA AAC GTG TTC -3′	C33H5.4
C33H5.4_Seq3	5′ - GAC ACG TTC CAT ACC GCG -3′	C33H5.4
C33H5.4_Seq4	5′ - AGC AGT TCT ACA TTC GAA TGC A -3′	C33H5.4
C33H5.4_Seq5	5′ - TGC TCC AGG GAG AAA TTG TC -3′	C33H5.4
C33H5.4_Seq6	5′ - GGC CTC ATT CGA TCT CTC G -3′	C33H5.4
C33H5.4_Seq7	5′ - GGC AGA GCC TGG CTG AGA-3′	C33H5.4

Table 2-2. Primers generated and used for sequencing of candidate genes.

2.4. SNIP-SNP mapping

Single nucleotide polymorphisms (SNPs) are detectable at high frequency between two wild-type variants of *C. elegans* (Hawaiian CB4856 and Bristol N2). The relatively even distribution of these polymorphisms is the basis for SNP mapping. By creating worms that are heterozygous for N2 and CB4856 DNA and allowing them to self-fertilize, generating recombinants homozygous for the SNP locus, one is able to narrow down the location of the crossover event (Wicks *et al.,* 2001). After determining whether or not the recombinant worm contains the mutation of interest, it is possible to resolve a relative position for the mutation (Figure 2-3). Many of the polymorphic sites are detectable only with subsequent restriction digestion of the PCR products; these SNPs are referred to as SNIP-SNPs (Wicks *et al.*, 2001).

Primer Name	Primer Sequence	Target	R.E.
pkp4080_left	5′ - AAC CTG TAC CTT GTT CAC CGC -3′	pkp4080	NsiI
pkp4080_right	5′ - TCA GCG AGA AAA TAG ACA TCG -3′	pkp4080	
F20C5_left	5′ - AGC CAA TGA AAA CTG GGT TG -3′	Snp_F20C5[1]	LweI
F20C5_right	5′ - TTG CTG ATT TGG CCT TCT TC -3′	Snp_F20C5[1]	
F08B4_left	5′ - ATC GTG ATT CCa ACA CCA GA -3′	Snp_F08B4[1]	HphI
F08B4_right	5′ - CAT GCT CGA AAA GGC ATA AA -3′	Snp_F08B4[1]	
pkp4079_left	5′ - AGA TTT GCC AAT TCC AAG TAG C -3′	pkp4079	MboI
pkp4079_right	5′ - CAG AAC AAT GAC CGA GTC GAG -3′	pkp4079	
M116[4]_left	5′ - GGG TCT ACG TGG CTT CTC AT-3′	Snp_M116[4]	BseNI
M116[4]_right	5′ - TCT CGC CTC TCC CAG TAG AT -3′	Snp_M116[4]	
pkp4078_left	5′ - TAT TCC AGT TTG CGA GAA TCC -3′	pkp4078	TaqI
pkp4078_right	5′ - TTT CGT GCT CAT CCA CGT G -3′	pkp4078	
pkp4038_left	5′ - AAT TCA GGT TCC TGC TTG CG -3′	pkp4038	HinFI
pkp4038_right	5′ - TCC GAA ACC AAT CGC CTA AG-3′	pkp4038	

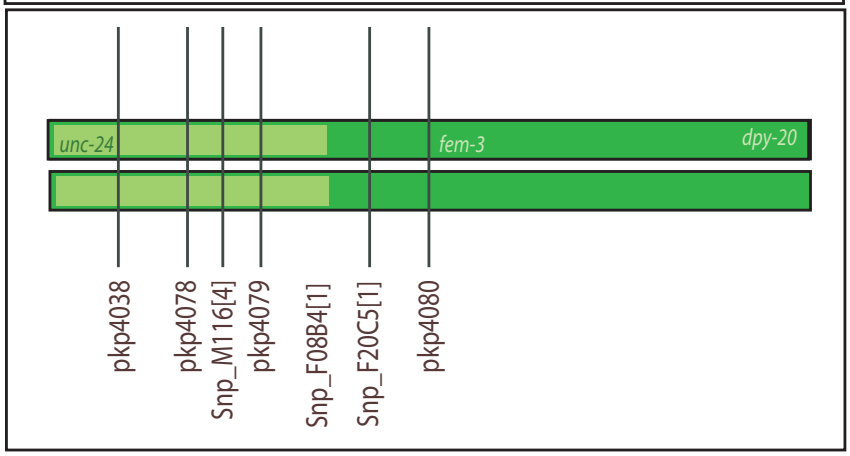

Figure 2-2. Primer sequences and SNIP-SNP locations. Top: PCR primer sequences and respective restriction enzymes (R.E.s) for SNP detection. Bottom: Physical location of SNIP SNPs between *unc-24* and *fem-3*.

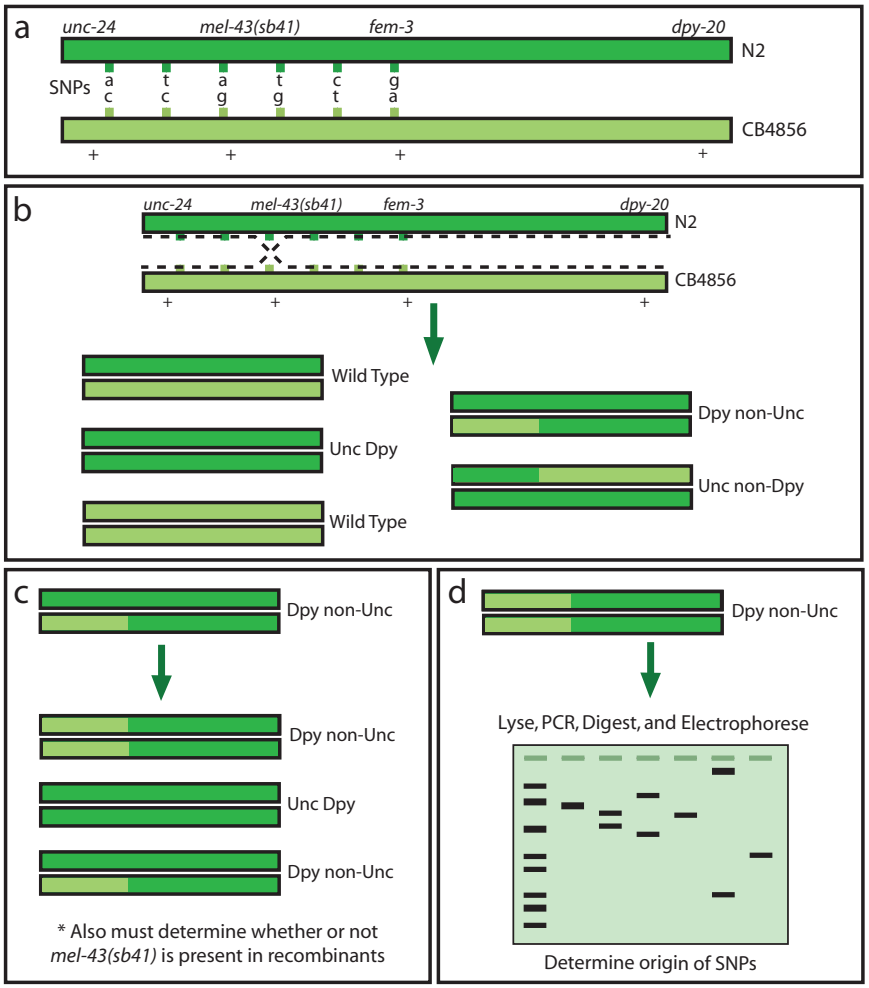

Figure 2-3. Mapping a mutation with SNIP-SNPs. a. Regularly spaced single nucleotide polymorphisms exist between two wild-type strains of *C. elegans*. The mutation of interest is flanked by two recessive visible markers to allow detection of crossover events from both directions. b. Placing the mutant chromosome over a CB4856 chromosome and allowing the hermaphrodite to self-fertilize will regenerate the parental heterozygotes and homozygotes (left) and rarely will produce detectable recombinants that have crossed out one of the visible markers (right). c. By picking all recombinants to individual plates and allowing them to self-fertilize, it is possible to obtain the homozygous recombinant chromosome, while at the same time determining whether or not the recombinant worms still contain the mutation. One quarter of the recombinant progeny generated from this event will be homozygous for the recombinant chromosome. d. After lysis and PCR of single worms, the solution is digested with an appropriate restriction enzyme and the products are resolved by agarose gel electrophoresis.

2.5. Two- and three-factor mapping

For mapping experiments, it was necessary to create unique heterozygotes that would allow recombinant worms to be detected in a background of parental phenotypes. In all cases, the original *mel-43(sb41) dpy-20* chromosome was placed *in trans* to a chromosome that contained two visible markers. Recombinant animals were picked to individual plates and tested for the presence of *mel-43(sb41)*. By calculating the frequency of certain recombinant events, it was possible to estimate a map location for *mel-43*.

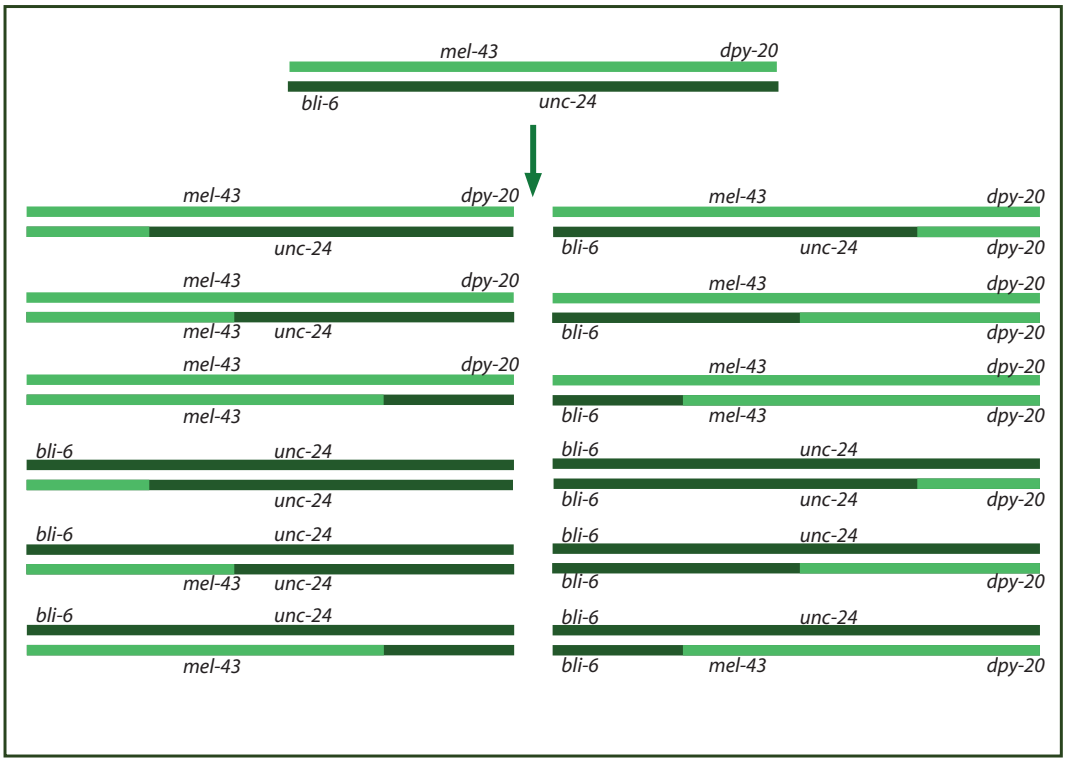

Figure 2-4. Genetic mapping of *mel-43* on chromosome IV. Mapping heterozygote and expected F1 recombinant progeny from self-fertilization, assuming *mel-43* resides between *bli-6* and *unc-24* and only one recombinant chromosome is contributed to each F2 embryo.

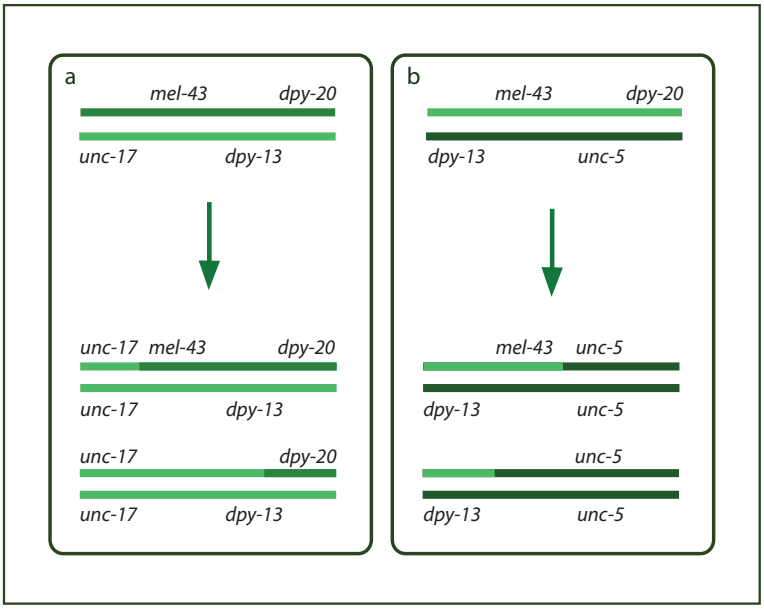

Figure 2-5. Mapping *mel-43* relative to morphological markers on chromosomes IV. a. Assuming *mel-43* is between *unc-17* and *dpy-13*, crossovers in this region will produce detectable Uncs that sometimes are Mel (maternal-effect embryonic lethal). b. Assuming *mel-43* is between *dpy-13* and *unc-5*, crossovers in this region will produce detectable Uncs that sometimes are Mel.

2.6. Deficiency characterization and mapping

In order to generate *mel-43(sb41)/mDf9* worms, *mel-43(sb41) dpy-20*/+ males were crossed into the balanced deficiency strain DR684 (*mDf9/nT1*). All outcrossed hermaphrodites generated in this cross were categorized into four genotypes, as detailed below (Figure 2-6). These hermaphrodites were allowed to self-fertilize at 15°C and then hatching levels were recorded. In order to ensure that viable eggs were not miscounted as dead eggs, hermaphrodites were transferred to new plates one day prior to scoring eggs and progeny.

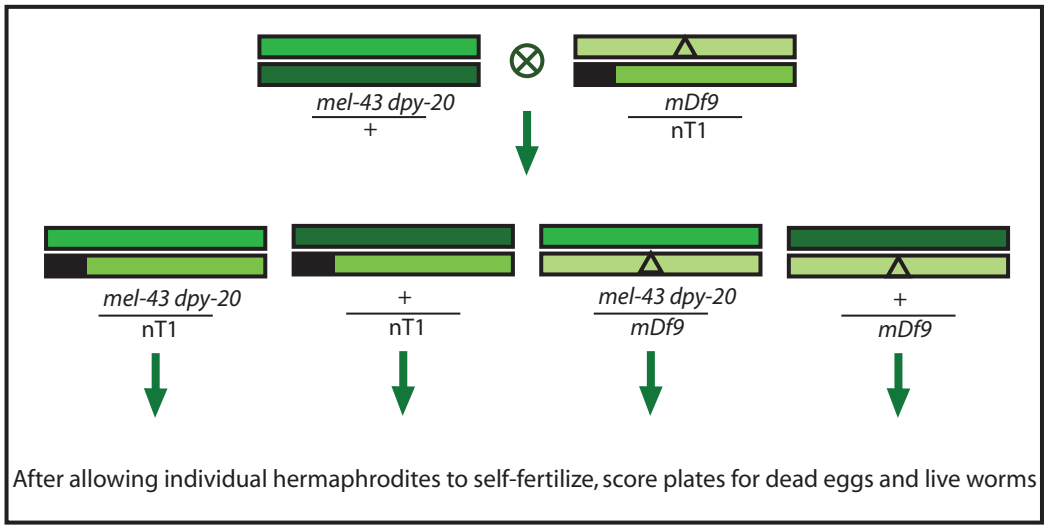

Figure 2-6. Crossing scheme to place *mel-43(sb41) in trans* to a deficiency in the region. Four genotypes are produced from the cross and are morphologically indistinguishable. F1 hermaphrodites are allowed to self-fertilize and then plates are scored for embryonic lethality. If the deficiency fails to complement *mel-43(sb41)*, it is expected that an exceptionally high degree of embryonic lethality will result.

2.7. Immunofluorescence

Between 20 and 30 gravid hermaphrodites were picked into 5 µL of water on a cover slip where they were dissected with a needle to allow the embryos to spill out. Polylysine-coated slides were placed over the coverslips and immediately frozen in liquid nitrogen. A razor blade was used to flick the coverslip off of the slide in order to crack the eggshells and allow antibodies to penetrate the embryos. The slides were fixed in ice cold Methanol for 15 minutes, at which time they were transferred to PBS for 5 minutes. The embryos were blocked with PBS and 25% goat serum for 30 minutes and then

incubated with the Primary Antibody solution (5% blocking solution, 0.01% Triton-X-100, Mouse anti α-Tubulin (1 µg/mL), and the relevant rabbit anti worm specific antibody (1 µg/mL) in PBS) for 60 minutes in humid conditions. Slides were washed in PBS twice for 10 minutes each and then the Secondary Antibody solution (5% blocking solution, 1% Triton-X-100, 1 µg/mL α-mouse, 1 µg/mL α-rabbit) was applied for 60 minutes in a dark humid chamber. Secondary antibodies covalently linked to one of three fluorophores (Alexa488, Alexa546, Alexa647) were used for visualization via fluorescence microscopy (Molecular Probes). The secondary antibody solution was aspirated from the slides and DAPI was applied for 5 minutes in a dark humid chamber. The slides were washed for 5 minutes in PBS twice and then the embryos were mounted in 8 µL mounting media (0.5% p-phenylenediamine, 20 mM Tris-Cl, pH 8.8, 90% glycerol). A coverslip was placed over the sample and sealed with nail polish.

Images were acquired using Volocity® Acquisition software on an Olympus IX81 motorized inverted microscope fitted with a Yokogawa CSU-10 spinning disc confocal head. Multiple image planes were acquired for each embryo, at an increment of 0.2 µm, for a total depth of approximately 30 µm (although this was dependent on the specific embryo). Tiff files were imported into and analyzed using MetaMorph® software. Uninformative planes were removed from projections of Tiff stacks in order to enhance the image.

2.8. *Ex-utero* confocal imaging

Between three and five worms were dissected on a coverslip in egg buffer (118mM NaCl, 48mM KCl, 2mM $CaCl_2$, 2mM $MgCl_2$ 25mM HEPES, pH 7.3, 340 mOsm). The coverslips were inverted onto 2% agarose pads on slides and the slides were viewed using differential interference contrast (DIC) microscopy. Time lapse DIC images were acquired using a 60X oil objective lens on an Olympus IX81 motorized inverted microscope equipped with a Yokogawa CSU-10 spinning disc confocal head. MetaMorph® software was used for measurements of embryo length.

2.9. *In-utero* confocal imaging

Between three and five worms were picked into M9 solution (22mM KH_2PO_4, 42mM Na_2HPO_4, 85mM NaCl, 1mM $MgSO_4$) containing 2mM tetramisole to immobilize the worms prior to imaging (approximately 5 minutes). Tetramisole is an acetylcholine agonist that allows the normal metabolic and developmental processes to occur while resulting in paralysis of the adult worm (Aceves *et al.,* 1970). For this reason, it is also useful as an antihelmenthic. After the worms ceased movement, the coverslip was mounted on a freshly prepared 2% agarose pad and imaged using a 60X oil immersion objective. Images were acquired between 20˚C and 22 ˚C.

After nuclear envelope breakdown was observed in the oocyte, single DIC images were acquired alternately with fluorescence stacks. This process was repeated every 20-30 seconds until the embryo divided. This allows the morphology of the embryo to be observed simultaneously with the cytoskeletal phenotype, which greatly aids in staging embryos. The fluorescence image stacks were projected and the projections were used to build a movie.

For timing measurements, landmarks of spermatheca exit, polar body I extrusion, polar body II extrusion, and cell cleavage were used to measure the rate of progression for meiosis I, meiosis II, and mitosis, respectively.

For fluorescence measurements, integrated intensity was calculated for projected stacks at each timepoint using a set region of measurement. In order to account for background photobleaching, integrated intensity was also calculated for a multicellular embryo in the uterus and then a ratio of fluorescence over time was determined.

3. Results

3.1. Observed hatching levels in *mel-43(sb41)* strains

mel-43(sb41) is a maternal-effect embryonic lethal (Mel) mutation. Contrary to non-Mel mutations, it is the mother's genotype that determines the phenotype of the animal. An important implication of this with regards to mapping is that animals have to be followed through two generations in order to determine the genotype. Because *mel-43(sb41)* is also temperature-sensitive and semi-dominant, the hatching rates for *mel-43(sb41)* homozygotes and heterozygotes vary at the permissive and restrictive temperatures (Figure 3-1).

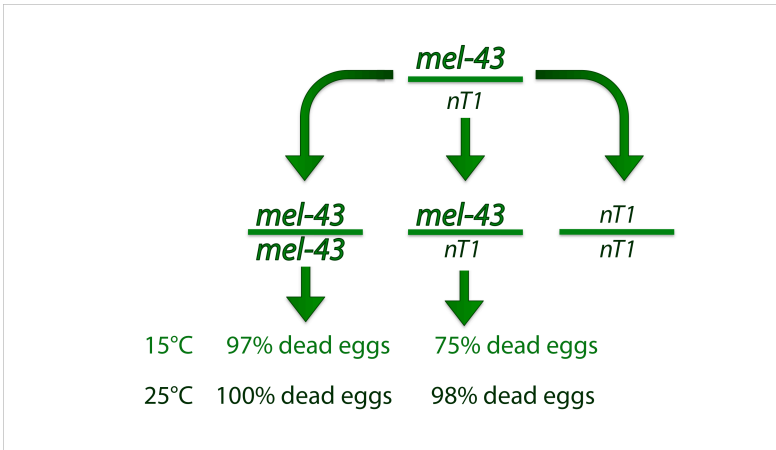

Figure 3-1. Maternal-effect embryonic lethal (Mel) phenotype of *mel-43(sb41)*. *mel-43(sb41)* is balanced over a translocation chromosome, *nT1*. Progeny from the balanced heterozygote include *mel-43(sb41)* homozygotes, *mel-43(sb41)* heterozygotes and *nT1* homozygotes. The *nT1* chromosome contains a recessive lethal marker and therefore *nT1* homozygotes are inviable. *mel-43(sb41)* homozygotes and heterozygotes are both viable, and the Mel phenotype is observed in the next generation.

At the permissive temperature of 15°C, *mel-43(sb41)* homozygotes result in 97% dead eggs and balanced heterozygotes result in 75% dead eggs. A portion of the lethality arising from the heterozygote is due to inherent zygotic lethality in the *nT1* translocation, and observation of *mel-43(sb41)/+* heterozygotes at 15°C (24.5% lethality) suggests that the lethality contributed by the nT1 translocation is 66.9%. At 25°C, *mel-43(sb41)* acts dominantly and balanced heterozygotes result in 98% dead eggs, whereas *mel-43(sb41)* homozygotes result in complete maternal-effect embryonic lethality.

3.2. Mapping *mel-43*

In preparation for SNIP-SNP mapping, a heterozygous worm containing *mel-43(sb41) dpy-20* on one chromosome and *unc-24* on the other chromosome was created. Ultimately the goal was to obtain a recombinant animal containing *unc-24 mel-43(sb41) dpy-20* on one chromosome. Individual Uncs were allowed to self-fertilize at 25°C and those that were Mel (indicating at least one copy of *mel-43(sb41)* and two copies of *unc-24*) were down-shifted to 15°C to rescue the recombinant chromosome. Over 5% of Unc F1 progeny were Mel at 25°C: based on the predicted map location for *mel-43* being 3.67, and *unc-24* residing at 3.51, less than 0.2% of F1 progeny were expected to contain *unc-24* and *mel-43(sb41)* on the same chromosome. The majority of F1 Mel Uncs were not able to be rescued upon downshift to 15°C; the one

animal that produced a few viable F2 progeny was maintained and determined to be lacking *dpy-20*.

In the event that temperature was having an unexpected effect resulting in an exaggeration of *unc-24 mel-43(sb41)* recombinant frequency, the screen was redesigned. From the heterozygous P1 hermaphrodite (*mel-43(sb41) dpy-20/unc-24*), all F1 Uncs were individually set up at 15°C. Those that produced Unc Dpy progeny were tested for the presence of *mel-43(sb41)*. Out of over 1400 F1 Unc progeny screened, 2% satisfied the requirement of producing Unc Dpy F2 progeny, consistent with the known map distance between *unc-24* and *dpy-20* (1.7). 0 out of 29 recombinant animals were Mel at 25°C. Additionally, one Unc that was set up at 15°C was Mel (and therefore contained 2 copies of *mel-43(sb41)*) but did not produce Unc Dpy progeny. These data prompted a re-evaluation of the proposed map location for *mel-43*: if *mel-43* is indeed between *unc-24* and *dpy-20*, double crossovers would explain the two incidents of Unc Mel non-Dpy worms. However, since the single crossover was never observed, it is more likely that *mel-43* was initially mapped incorrectly (see Discussion).

In order to determine which region of chromosome IV *mel-43* resides on, a series of mapping experiments were designed. Initially, a strain of the genotype *mel-43(sb41) dpy-20/ bli-6 unc-24* was created to perform a large-scale mapping experiment. 1421 F1 progeny were picked to individual plates and genotyped (Figure 3-2). Using the recombination frequency between

mel-43 and *dpy-20*, *mel-43* was mapped to a location of 0.06 on chromosome IV (Figure 3-2).

In order to refine this map position, two new mapping heterozygotes were created: *unc-17 dpy-13/ mel-43(sb41) dpy-20* and *dpy-13 unc-5/ mel-43(sb41) dpy-20*. Unc non-Dpy recombinants were tested at 25° for the presence of *mel-43(sb41)*. 27 recombinant progeny from two separate experiments places *mel-43* to the left of *dpy-13* and to the right of *unc-17* at a position of -1.38 on chromosome IV (Figure 3-3a,b).

a

	Number Scored	Dpy non-Mel	Mel non-Dpy
bli-6 unc-24/ mel-43 dpy-20	644		
bli-6 unc-24/ bli-6 unc-24	322		
mel-43 dpy-20/ mel-43 dpy-20	376		
bli-6 unc-24 / bli-6 dpy-20	4	4	
mel-43 dpy-20 / mel-43	6		6
bli-6 unc-24 / bli-6	3		3
unc-24 dpy-20 / mel-43 dpy-20	8	8	
mel-43 dpy-20 / dpy-20	19	19	
mel-43 bli-6 unc-24 / mel-43 dpy-20	15		15
mel-43/ mel-43 dpy-20	17		17
bli-6 unc-24 / bli-6 unc-24 dpy- 20	7	7	
Total	1421	38	41

b

Figure 3-2. Mapping experiment to determine relative location of *mel-43* on chromosome IV. a. inferred parental genotypes (green), recombinants (black) and their respective genotypes. b. shows the proposed location for *mel-43* based on these mapping data.

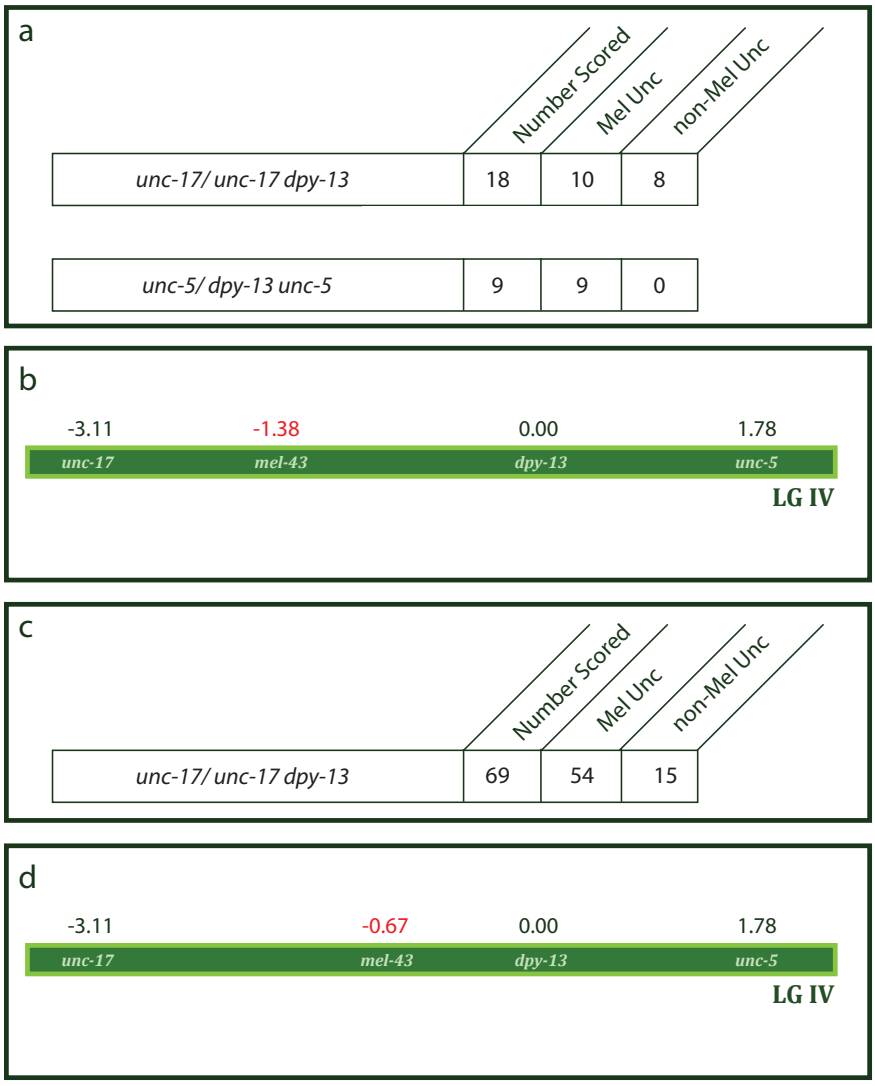

Figure 3-3. Mapping experiment to position *mel-43* on one side of *dpy-13*. a. shows the total number of recombinants scored and the Mel status of the recombinants. b. shows the predicted map location for *mel-43* based on these mapping data. c. shows the total number of recombinants scored in the scaled-up screen and the Mel status of the recombinants. d.shows the predicted location of *mel-43* based on data in c.

In order to refine the location of *mel-43* between *unc-17* and *dpy-13*, additional *mel-43(sb41) dpy-20/unc-17 dpy-13* heterozygotes were set up, allowed to self fertilize, and F1 progeny were tested for the presence of *mel-43(sb41)*. Out of 69 total recombinants tested for the presence of *mel-43(sb41)*, 54 were determined to be Mel and 15 were determined to be non-Mel. Calculation of recombination frequency places *mel-43* at -0.67 on chromosome IV, between *unc-17 and dpy-13* (Figure 3-3).

3.3. Deficiency analysis and mapping

The placement of a deficiency over a mutation can provide at least two pieces of information. First, the deficiency allows a classification of the mutant behavior; weak loss-of-function alleles usually display an increase in the severity of the phenotype when placed over a deletion, whereas null mutations usually display a similar phenotype. Second, if the deficiency breakpoints are known, then the placement of the mutation within the deficiency provides information about the physical location of the mutation.

In *C. elegans*, many large-scale deficiencies exist that cover a large portion of the genome. On chromosome IV, there are two deficiencies that span the *dpy-13* locus and could potentially encompass the *mel-43* region: *mDf9* and *mDf4*. *mDf9* is the larger of the two with predicted breakpoints at -.969 and

2.155[1]. In order to determine if *mDf9* deletes the *mel-43* locus, and what effect the deficiency has on the phenotype, *mel-43(sb41)* was placed *in trans* to *mDf9* and plates were scored for embryonic lethality (Figure 3-4). If *mDf9* deletes the *mel-43* locus, and *mel-43(sb41)* is a complete loss-of-function mutation, a level of embryonic lethality similar to *mel-43(sb41)* homozygotes is expected, resulting from a synergistic contribution. If *mDf9* does not delete the *mel-43* locus, the level of embryonic lethality will be the product of lethality due to *mel-43(sb41)* alone and *mDf9* alone.

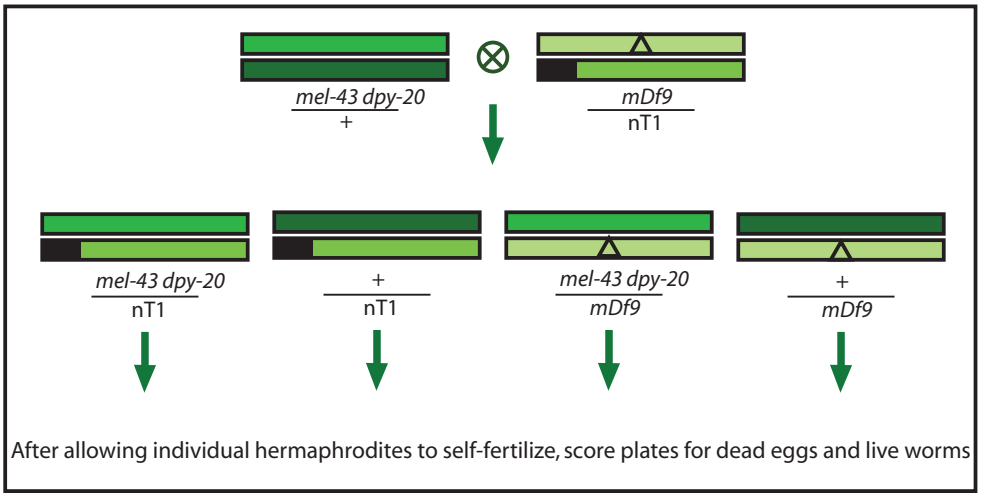

Figure 3-4. Deficiency *mDf9* crossing scheme. Male worms heterozygous for *mel-43(sb41) dpy-20 are* crossed to hermaphrodites heterozygous for *mDf9*. Four genotypes are expected, including *mel-43(sb41) dpy-20/mDf9*. Analysis of embryonic lethality of *mel-43(sb41) dpy-20/mDf9* provides insight into the genetic behaviour of *mel-43(sb41)*.

[1] Using the 'first undeleted locus' to determine breakpoints results in a more conservative estimate of the rearrangement size: -1.75 to 2.45.

After crossing *mel-43(sb41)/+* heterozygotes to the strain DR684, containing the deficiency *mDf9/nT1*, outcrossed F1 progeny were plated and allowed to self-fertilize at 15°C. Due to a lack of dominant visible markers, it was impossible to genotype the F1 worms directly. Therefore plates were 'blindly' scored for embryonic lethality. In order to score egg viability, the gravid hermaphrodites were transferred off of the plates one day prior to scoring. Additionally two control DR684 hermaphrodites were plated and scored to measure embryonic lethality in *mDf9/nT1* worms. A total of 22 F1 hermaphrodites were plated individually and their progeny scored. DR684 control hermaphrodites exhibited 72.5% embryonic lethality, suggesting that the region deleted by mDf9 is slightly haplo-insufficient. In the experimental group, embryonic lethality ranged from 42.6% to 100% (Figure 3-5). Additionally, *mel-43(sb41) dpy-20/nT1* was created and scored: heterozygotes resulted in 67% embryonic lethality.

After determining embryonic lethality values for *mel-43(sb41) dpy-20/nT1, mDf9/nT1,* and *mel-43(sb41)/+* heterozygotes, it was possible to back-calculate the amount of lethality contributed by each chromosome, assuming complete independence. These values were used to predict the expected percent embryonic lethality for the expected genotypes resulting from the cross between *mel-43(sb41) dpy-20/+* and *mDf9/nT1* (Table 3-1).

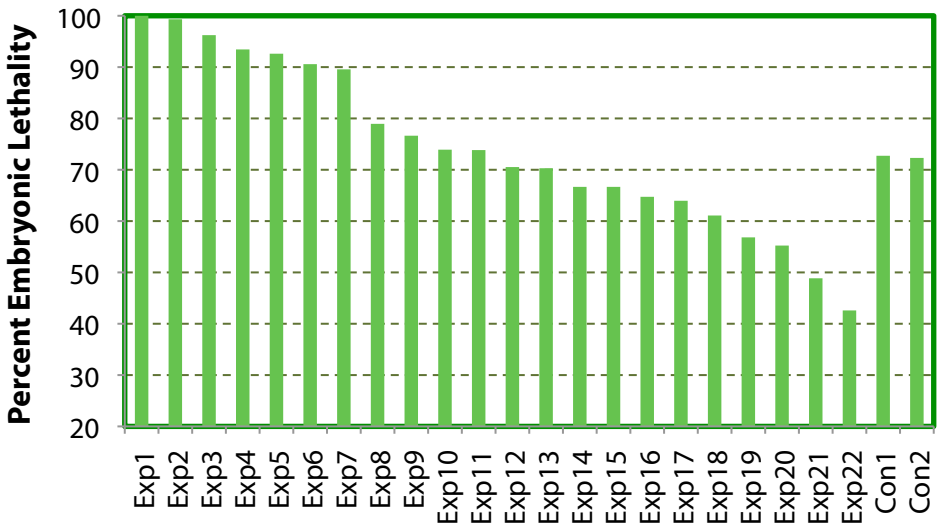

Figure 3-5. Range of embryonic lethality percentages observed from analysis of 22 F1 progeny from a *mel-43(sb41)*/+ x *mDf9/nT1* cross. F1 hermaphrodites were blindly scored at 15°C. Con1 and Con2 refers to balanced mDf9/nT1 hermaphrodites that were set up at 15°C.

Genotype	Embryonic Lethality (15°C)
mel-43 dpy-20/+	23.5%
mel-43 dpy-20/nT1	67%
mDf9/nT1	72.5%

Genotype	Expected Embryonic Lethality (15°C)*
mel-43 dpy-20/nT1	67%
mel-43 dpy-20/mDf9	51%
+/nT1	57%
+/mDf9	36%

* Calculated using the formula a × b = c, where a represents survival due to chromosome A, b represents survival due to chromosome B, and c represents survival of the heterozygote A/B. Lethality = 1- % survival.

Using known lethality of mDf9/nT1, mel-43/nT1 and mel-43/+, values were calculated for expected deficiency cross progeny.

Table 3-1. Expected embryonic lethality values for deficiency cross F1 progeny. Assuming complete independence and no synthetic interactions, expected levels of embryonic lethality were calculated based on measured values of known genotypes.

A total of four genotypes were expected from the cross between *mel-43(sb41)* heterozygotes to balanced deficiency hermaphrodites (Figure 3-4). Therefore, it was possible to allocate all 22 hermaphrodites into four batches. Using natural 'breaks' observed in the data, four groups were compiled (Figure 3-6). One of these groups had an extremely high percent lethality, 93.62%. A comparison to observed *mel-43(sb41)/mel-43(sb41)* embryonic lethality values at 15°C shows that the values are very similar (Figure 3-7).

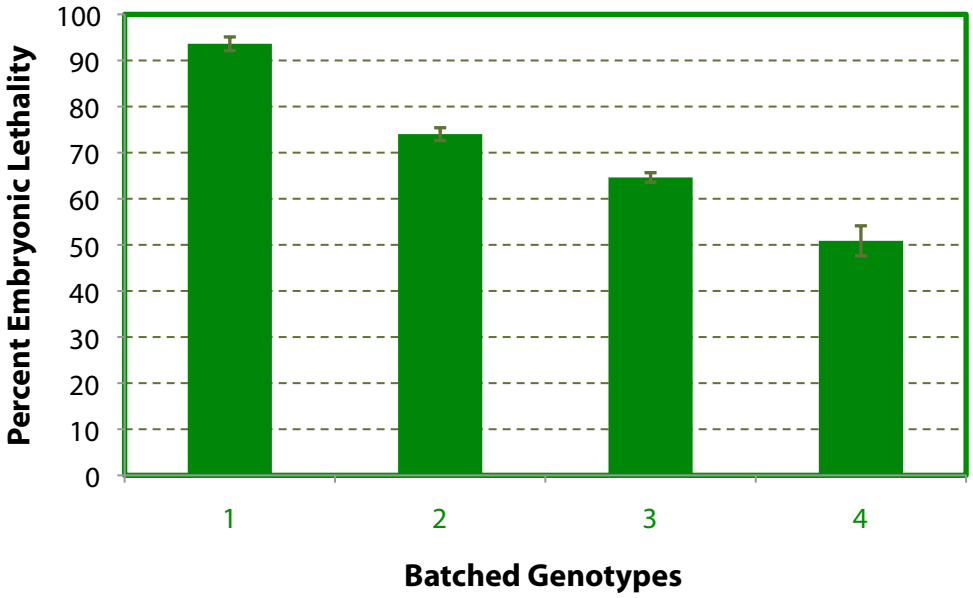

Figure 3-6. Batching of progeny according to embryonic lethality levels (Figure 3-4). Naturally-occurring breakpoints in the data were used to batch the 22 hermaphrodites into 4 groups, blindly corresponding to the 4 genotypes expected. Standard error was calculated as a measure of significance (error bars).

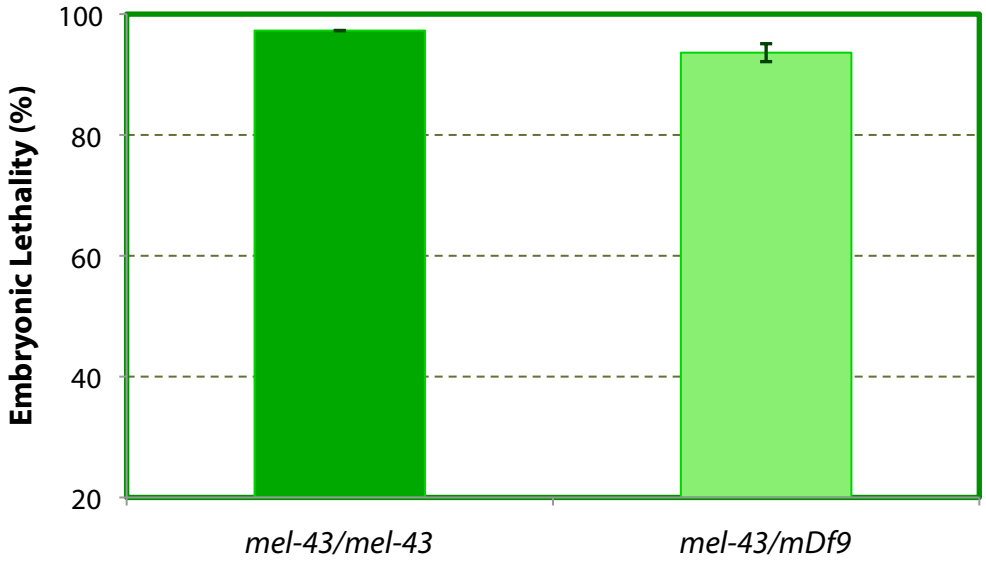

Figure 3-7. Comparison of homozygous *mel-43(sb41)* embryonic lethality levels to suspected *mel-43(sb41)/mDf9* embryonic lethality levels. Standard error was calculated as a measure of significance (error bars).

In summary, *mel-43(sb41)* heterozygotes were crossed to a strain heterozygous for *mDf9*, a deficiency that spans the predicted *mel-43* locus. F1 hermaphrodites were set up on individual plates to self-fertilize and then embryonic lethality was scored. Because F1 progeny were blindly scored, they were batched into four classes, representing the four expected genotypes. Assuming complete independence, the highest embryonic lethality was expected from *mel-43(sb41)/nT1* at 67% (Table 3-1). One class had an exceptionally high degree of embryonic lethality (93.6%), and this was assumed to be *mel-43(sb41)/mDf9* because it was the only unknown, barring any synthetic interactions between chromosomal markers and rearrangements. Taking into account the extreme temperature sensitivity of

mel-43(sb41), when directly compared to homozygous *mel-43(sb41)* embryonic lethality, the values were very similar (Figure 3-7). Additionally, the values for *mel-43(sb41)/mDf9* are within the typically observed range for *mel-43(sb41)* homozygotes at 15°C (93-100%; not shown).

3.4. Sequencing of candidate genes

In the course of this study, a large portion of chromosome IV was visually scanned for candidate genes. Genes were selected as candidates based on the RNAi phenotype as reported in PhenoBank, sequence, and the predicted location of *mel-43*, which changed over the course of the study. Two genes, C28C12.2 and C33H5.4, fit the criteria for the identity of *mel-43*, in that they mapped to the same area of chromosome IV as *mel-43* at the time of sequencing and evidence suggested they had meiotic roles. Primers were designed to amplify overlapping sections of the respective coding sequences, and with the exception of a small region of C33H5.4 (due to primer design), both candidates were sequenced completely (Figure 3-8). C28C12.2 was sequenced in wild-type and homozygous *mel-43(sb41)* worms and no differences were detected. C33H5.4 was sequenced in homozygous *mel-43(sb41)* worms as well as in homozygous *sb41sb67* and *sb41sb69* worms (proposed *mel-43(sb41)* loss-of-function alleles; Mitenko *et al.,* 1997), and no differences were detected (Figure 3-8).

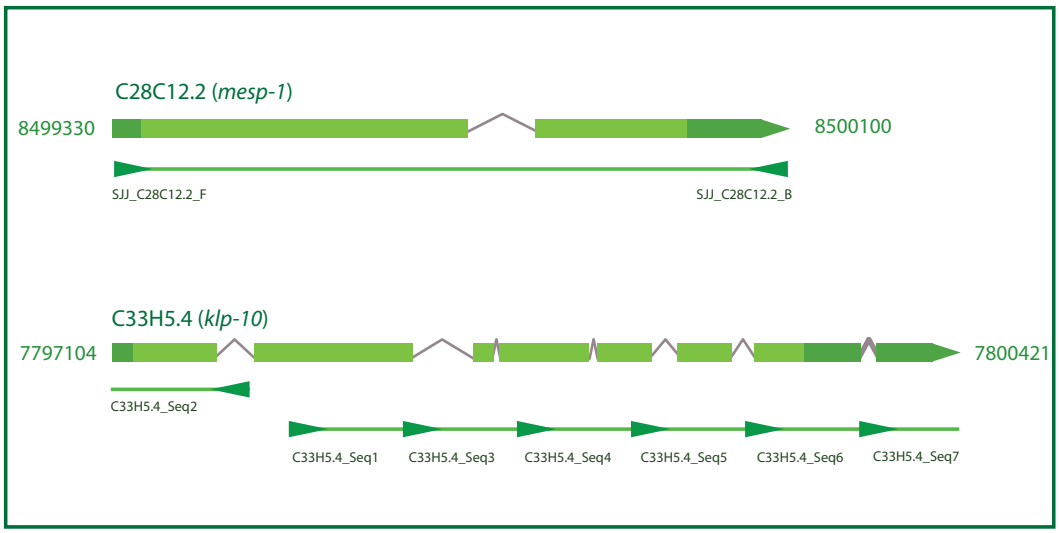

Figure 3-8. Diagram showing regions of two candidate genes that were sequenced. Primers used for sequencing are listed in Materials and Methods of this thesis.

3.5. Live imaging characterization of *mel-43(sb41)* embryos

As *mel-43(sb41)* has a prominent early embryonic cellular phenotype, phenotypic characterization is facilitated by a microscopy-based approach. Of particular interest is the single cell embryo and the cytoskeletal dynamics that occur within it. Using a strain containing *mel-43(sb41)* as well as a β-tubulin::GFP or histone::GFP fluorescent transgene, live imaging was used to characterize the microtubule cytoskeleton and DNA structure in *mel-43(sb41)* embryos (Figure 3-9).

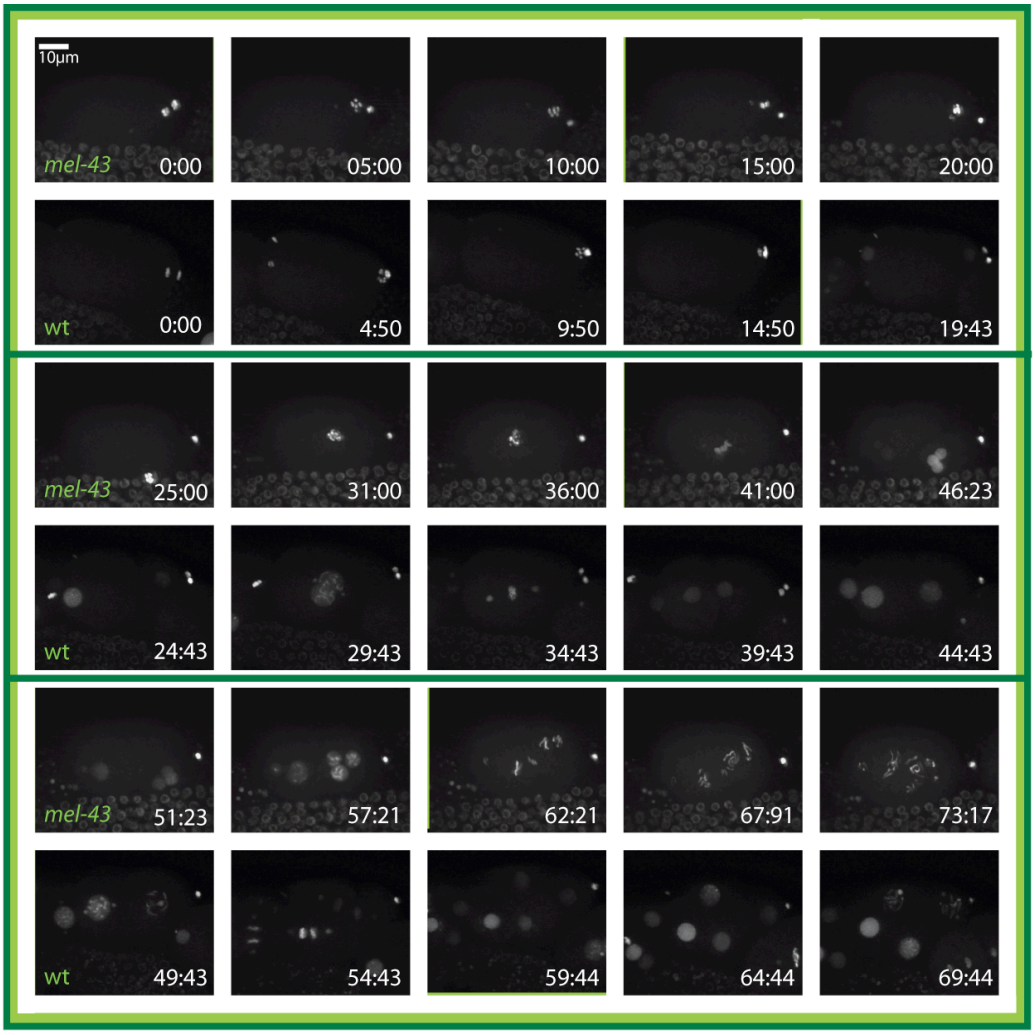

Figure 3-9. Comparison of DNA rearrangements in *mel-43(sb41)* embryos and wild-type embryos. ***mel-43(sb41)*** **embryos contain a fluorescent histone::GFP transgene and wild-type embryos contain a fluorescent histone::GFP transgene as well as a γ-Tubulin::GFP transgene. Time 0:00 marks the first meiotic anaphase. Following polar body extrusion, both *mel-43(sb41)* and wild-type embryos enter meiosis II. In *mel-43(sb41)* embryos, the second meiotic metaphase spindle is present at the same time (36:00) that wild-type embryos are in mitotic metaphase (34:43). This spindle eventually dissolves and multiple female pronuclei form (46:23 onwards in *mel-43(sb41)* embryos).**

3.6. *In-utero* timing of one-cell *mel-43(sb41)* embryos

Preliminary DIC characterization of the *mel-43(sb41)* phenotype suggested a severe early embryonic phenotype (Mitenko *et al*., 1997). In order to more closely examine the cytoskeletal structure of the embryo, spinning disc confocal fluorescence microscopy was used. In order to visualize the microtubule cytoskeleton, it was necessary to create a *mel-43(sb41)* strain that also expressed the β-tubulin::GFP marker (MAS88). The visualization of microtubules in this mutant background enabled an examination of microtubule defects as well as a precise staging of early cell-cycle event based on meiotic and mitotic spindle morphology, size and position.

Upon fertilization, a chitinous eggshell is synthesized and acts as an osmotic and physical protective barrier for the embryo, allowing manual dissection of the embryos from a gravid hermaphrodite into buffer for live imaging at high magnification. Eggshell deposition is not complete until after the first polar body extrusion, and it is difficult to preserve embryos prior to this time. It was previously observed that two-cell *mel-43(sb41)* embryos divide synchronously (Mitenko *et al.,*1997), suggesting that polarity establishment is incomplete and/or defective (this is also observed in *par-3* mutants; Gomes *et al.,* 2001). Fertilization, eggshell deposition, and meiosis are all necessary to establish polarity and it is therefore important to begin imaging at or prior to fertilization (Johnston *et al.,* 2006; Goldstein and Hird, 1996; Liu *et al.,* 2004). For this purpose, *in utero* imaging was used to observe

the passage of the oocyte through the spermatheca where it is fertilized, into the uterus where it completes a number of early cleavages. The 30 µm depth of the embryo and the unpredictability of the spindle movement and placement makes it difficult to capture all of the cellular events in a single focal plane. Therefore, fluorescence z-stack timelapse imaging was used in order to provide a complete view of embryonic structures over time. In addition, a single DIC image of the mid-plane was acquired at each timepoint. For all imaging, homozygous *mel-43(sb41)* homozygotes were used.

Initial analysis of *mel-43(sb41)*; β-tubulin::GFP embryos identified a potential delay in the first cell cycle and a failure to extrude a second polar body (Figure 3-10). Both *mel-43(sb41)* and wild-type β-tubulin::GFP embryos were imaged from nuclear envelope breakdown in the oocyte to first mitotic cleavage in the zygote. Interestingly, *mel-43(sb41)* embryos required an additional ten minutes to progress through these events when compared with wild-type. This is suggestive of a meiotic or mitotic cell cycle delay. To distinguish between these two possibilities, acquired movies were re-examined. Timepoints corresponding to the exit of the oocyte from the spermatheca, completion of meiosis I (first polar body extrusion), meiosis II (second polar body extrusion), and mitosis (cytokinesis) were recorded. In all cases (n=6), *mel-43(sb41)* embryos failed to extrude a second polar body. Often the meiotic metaphase spindle disintegrated before the oocyte pronucleus coalesced with the sperm pronucleus and underwent mitosis; for

these embryos, the meiosis II timepoint utilized was the meiotic spindle dissolution.

Using the values obtained, it was possible to determine the time that the embryos spent in meiosis I, meiosis II, and mitosis (Figure 3-11; Figure 3-12). A separate variance t-test was used to determine whether differences observed were significant. For the first time-point (exit from the spermatheca and extrusion of the first polar body) no statistically significant difference was observed between wild-type and *mel-43(sb41)* embryos ($P = 0.77$, $\alpha = 0.05$). The time elapsed between the first and second polar body extrusion, corresponding to meiosis II events, was on average thirteen minutes longer in *mel-43(sb41)* embryos, and was statistically significant ($P < 0.01$, $\alpha = 0.05$). The time elapsed between the second polar body extrusion and cleavage, corresponding to preparatory nuclear events and mitosis, was not significantly different between *mel-43(sb41)* and wild-type embryos.

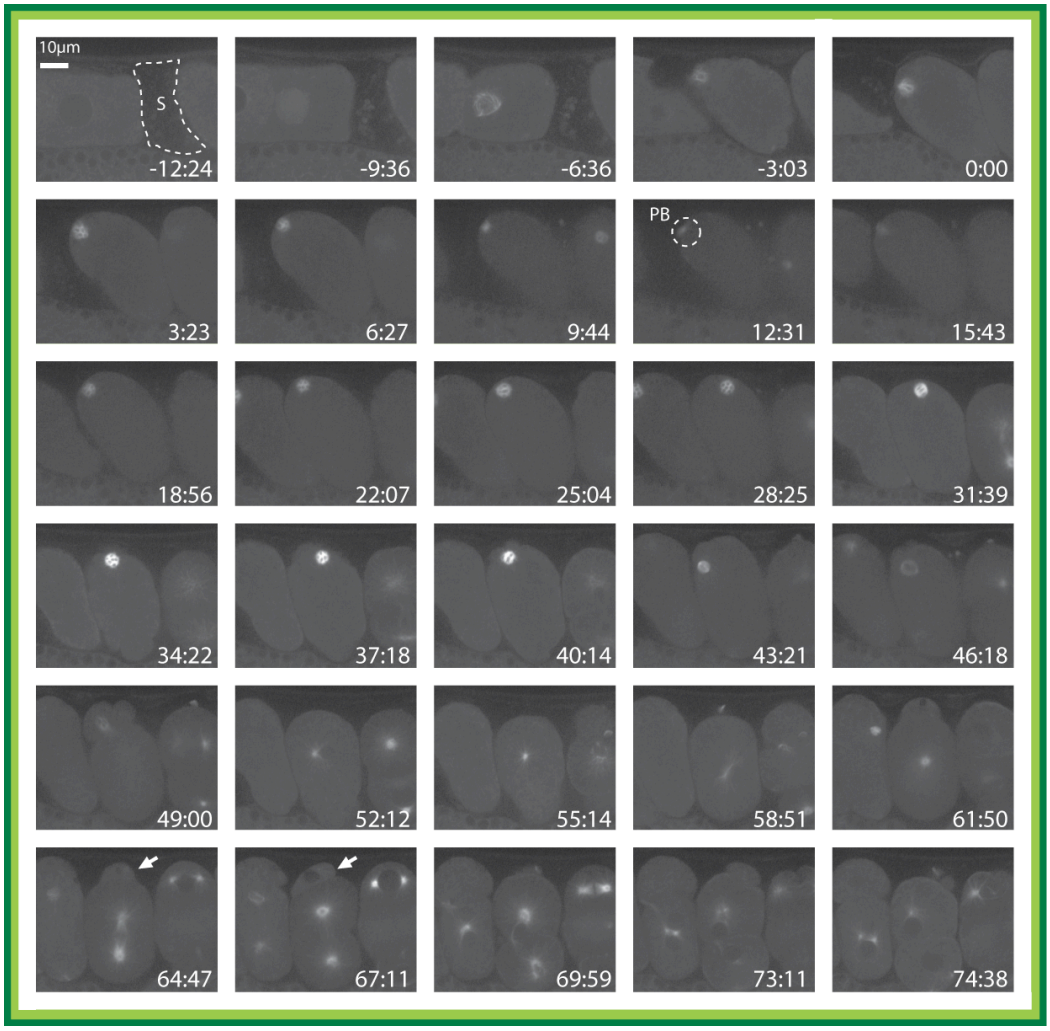

Figure 3-10. Timing of *mel-43(sb41)* embryos through the first cell cycle. Time 0:00 corresponds to spermatheca exit (S). At 12:31, the first polar body (PB) is extruded, representing the end of meiosis I. A meiosis II spindle subsequently forms and persists until 46:18 when it wanes in fluorescence and loses its structure. A mitotic spindle is produced and the embryo divides by 67:11. Arrows indicate cytokinetic defects typical of *mel-43(sb41)* embryos .

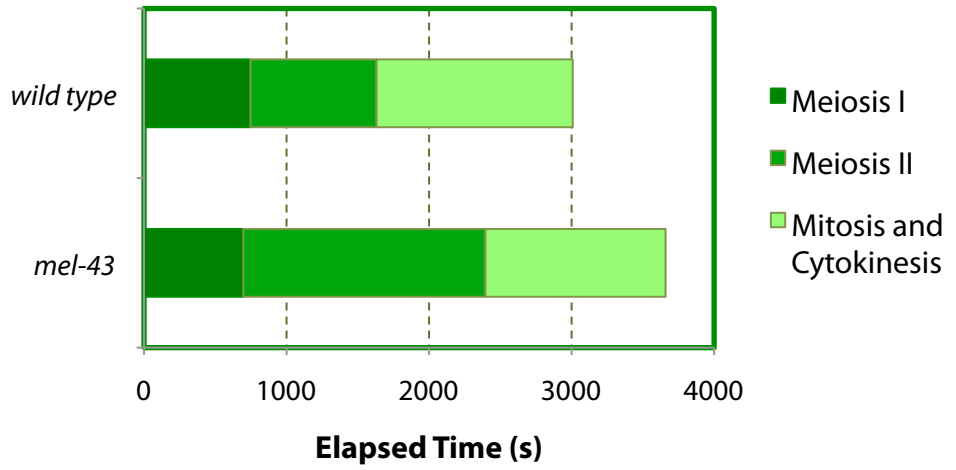

Figure 3-11. Total time elapsed in the one-cell embryo. Times are divided into meiosis I, meiosis II, and mitosis/ cytokinesis. 9 wild-type embryos and 6 *mel-43(sb41)* embryos were used for calculations.

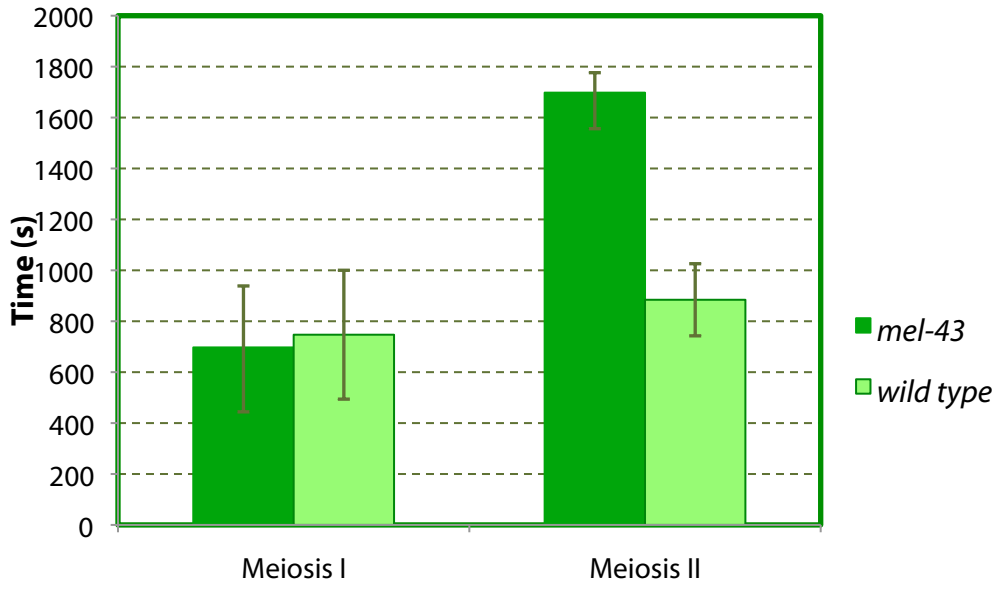

Figure 3-12. Duration of meiosis I and meiosis II in *mel-43(sb41)* and wild-type embryos. Embryos were imaged *in-utero*. Meiosis I is calculated from spermatheca exit to the first polar body extrusion. Meiosis II was calculated from the first polar body extrusion to the second polar body extrusion or dissolution of the meiotic spindle. 9 wild-type embryos and 6 *mel-43(sb41)* embryos were used for calculations. Standard error was calculated to determine significance (error bars).

3.7. Centrosomal maturation in *mel-43(sb41)* embryos

Early observations emphasized a defect in the meiosis to mitosis transition in one-cell embryos. One possibility for this defective transition is a premature or aberrant centrosomal maturation. For example, if centrosomes nucleate an extensive array of microtubules while the meiotic spindle is still present, these microtubules could physically interfere with the meiotic spindle and/or prevent proper segregation of meiotic chromatin. In order to determine whether centrosome maturation proceeds normally in *mel-43(sb41)* homozygotes, immunofluorescence was used to detect the localization of three centrosomal proteins: KLP-7, TAC-1 and γ-tubulin. KLP-7 is a kinesin-like protein that depolymerizes microtubules and localizes to kinetochores and centrosomes (Schlaitz *et al.,* 2007; Srayko *et al.,* 2005). TAC-1 is initially present at the meiotic spindle and localizes to the centrosome complexed with ZYG-9 in an AIR-1-dependent manner; it functions to regulate microtubule length (Le Bot *et al.,* 2003; Srayko *et al,* 2003). γ-tubulin forms a scaffold at the centrosome and stabilizes the minus ends of microtubules. No obvious defects were observed in *mel-43(sb41)* embryos immunostained for γ-tubulin (Figure 3-13). KLP-7 was detected at the sperm centrosomes (and kinetochores at metaphase) in both *mel-43(sb41)* and wild type embryos (Figure 3-14). TAC-1 appeared to be localized properly at the centrosomes in *mel-43(sb41)* and wild type embryos (Figure 3-15). In conclusion, no discernable differences were detected between *mel-43(sb41)* and wild type

embryos with respect to γ-tubulin, KLP-7, and TAC-1 localization at the centrosomes.

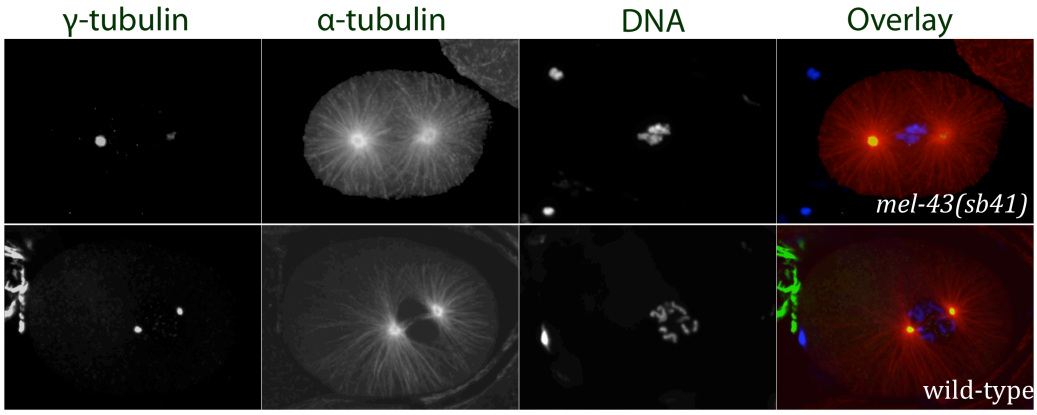

Figure 3-13. Immunofluorescence microscopy of *mel-43(sb41)*and wild type embryos detecting γ-tubulin, α-tubulin, and DNA in mitotic one-cell embryos.

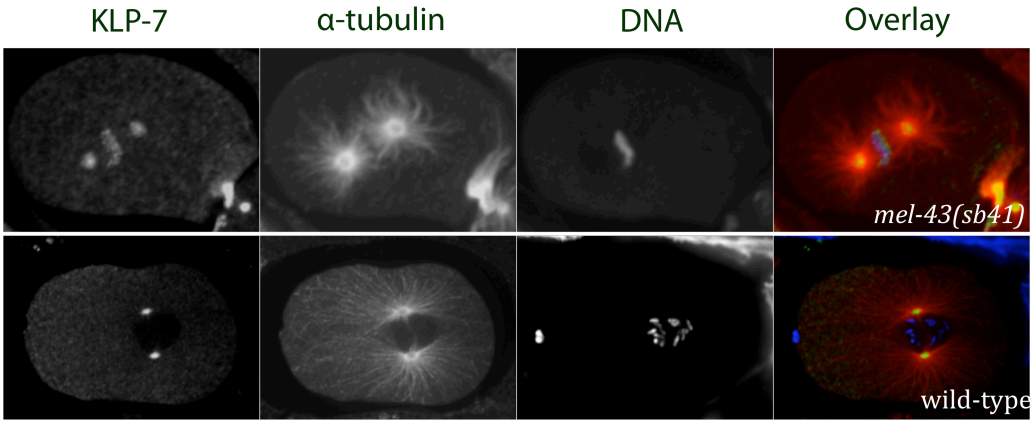

Figure 3-14. Immunofluorescence microscopy of *mel-43(sb41)* and wild type embryos detecting KLP-7, α-tubulin, and DNA in mitotic one-cell embryos.

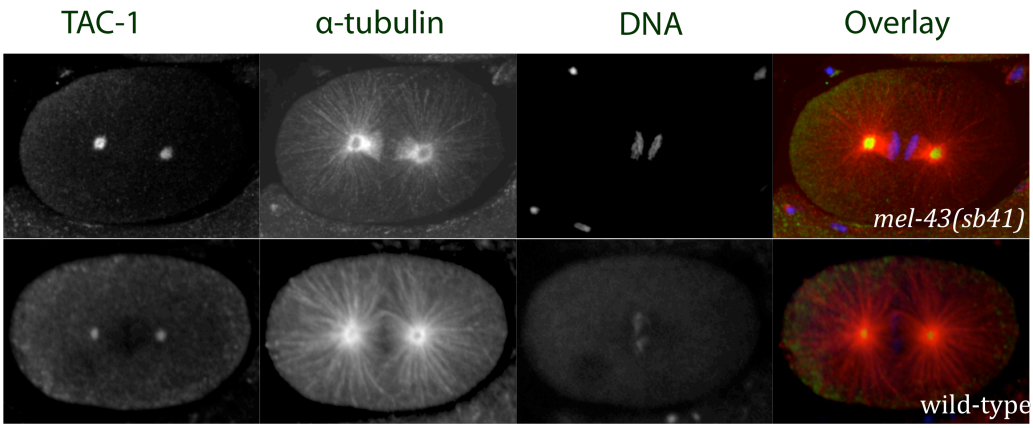

Figure 3-15. Immunofluorescence microscopy of *mel-43(sb41)* and wild type embryos detecting TAC-1, α-tubulin, and DNA in mitotic one-cell embryos.

3.8. Polarity establishment in *mel-43(sb41)* embryos

During mitotic metaphase and anaphase in the one-cell embryo, the mitotic spindle displaces towards the posterior, generating an asymmetric cleavage plane that produces a larger AB daughter cell and a smaller P1 daughter cell, which then go on to divide asynchronously. It was previously reported that two-cell *mel-43(sb41)* embryos fail to divide asynchronously (Mitenko *et al.,* 2007). Immunofluorescence analysis of two-cell *mel-43(sb41)* and wild type embryos confirms this (Figure 3-16).

Initial observation of *mel-43(sb41)* embyros highlighted a potential polarity defect, where single cell embryos appeared to divide symmetrically. In order to ascertain if *mel-43(sb41)* embryos are able to establish polarity and undergo a proper asymmetric first division, two techniques were employed:

immunofluorescence imaging of the polarity marker PAR-1, and measurements of the daughter cell lengths in two-cell embryos. In *C. elegans*, sperm entry initiates polarization along the anterior-posterior axis. This is a coordinated effort involving cortical rearrangements and spatial restriction of the maternally-provided PAR proteins. Proper polarity establishment is dependent on fertilization, eggshell secretion, and proper meioses and mitosis in the single cell embryo. PAR-1 is a kinase that becomes localized specifically to the posterior periphery of the embryo and therefore antibody staining against PAR-1 is diagnostic for proper establishment of the anterior-posterior (A-P) axis.

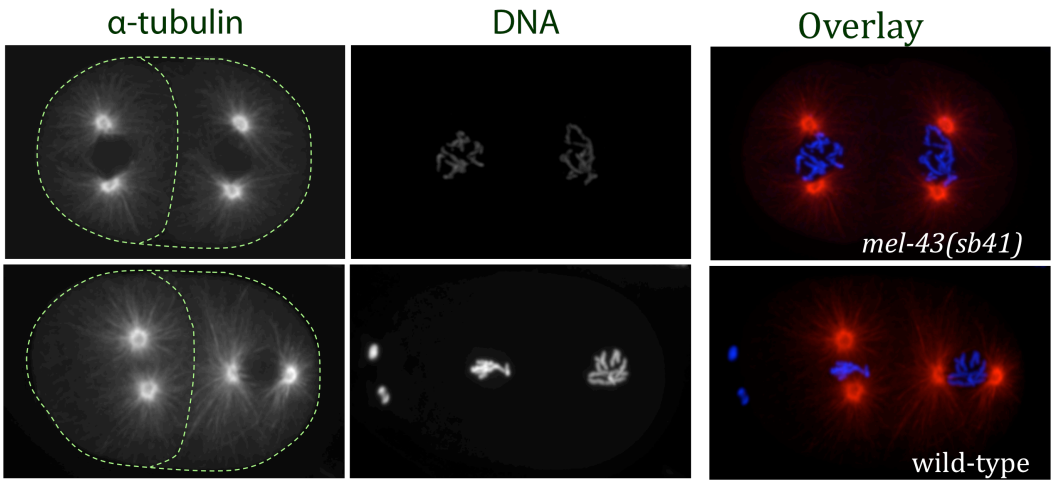

Figure 3-16. Two-cell *mel-43(sb41)* embryos divide synchronously. Immunofluorescence microscopy was performed on *mel-43(sb41)* and wild type embryos detecting α-tubulin and DNA.

Using a polyclonal antibody against PAR-1, homozygous *mel-43(sb41)* embryos were stained and imaged using fluorescence confocal microscopy. In wild-type embryos that establish polarity properly, PAR-1 is detected at the posterior periphery of the embryo from early mitosis onwards. In *mel-43(sb41)* embryos the location of PAR-1 varied: in addition to vast morphological defects observed in *mel-43(sb41)* embryos, PAR-1 staining was often absent at the cortex, aberrantly localized, or weakly present (Figure 3-17).

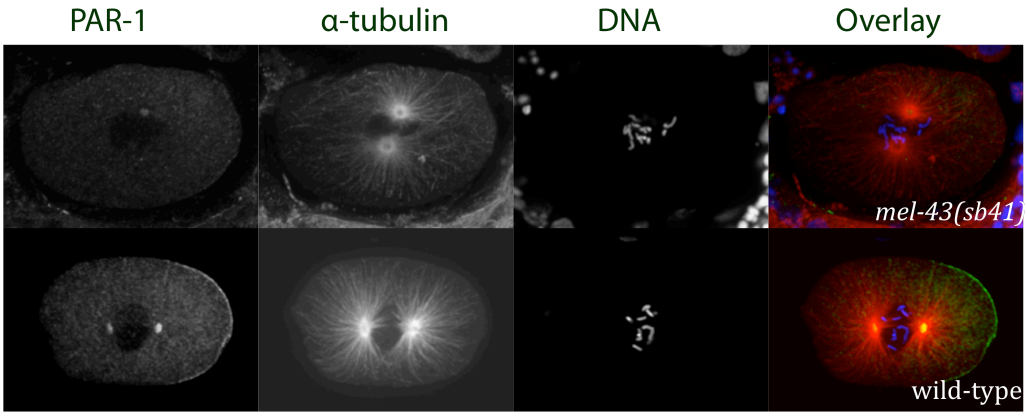

Figure 3-17. Immunofluorescence microscopy of *mel-43(sb41)* and wild type embryos detecting PAR-1, α-tubulin, and DNA in mitotic one-cell embryos. PAR-1 normally localizes to the posterior cortex in mitotic wild type embryos and is also detected at the centrosomes. In *mel-43(sb41)* embryos, PAR-1 is often absent from the cortex and faintly detected at the centrosomes, although a range of phenotypes was observed.

In order to confirm that the aberrant PAR protein localization observed is indicative of a genuine polarity defect, two-cell embryos were analyzed to determine whether or not an asymmetric first division had occurred. DIC images of *mel-43(sb41)* and wild-type embryos were acquired. Using the A-P

axis plane from single-cell embryos, distances from the anterior and posterior peripheries to the site of the first cleavage event were measured. It is impossible to confidently identify the AB and P1 daughter cells using DIC microscopy because polar bodies are not easily observed. Therefore, in order to objectively quantify the length differences between the two cells in an embryo, the deviation of the cleavage furrow from the centre of the embryo was calculated and represented as a percent of total embryo length (Figure 3-18). Ten embryos were measured for each of wild-type and *mel-43(sb41)*. In the wild-type embryos examined, the cleavage furrow was offset from the centre an average of 4.5% embryo length whereas in *mel-43(sb41)* embryos, this deviation was determined to be 1.4% embryo length (Figure 3-19). Standard error was calculated as a measure of significance (error bars). In summary, the cleavage furrow is displaced from the centre of the embryo to a lesser degree in *mel-43(sb41)* embryos than in wild-type embryos, suggesting that *mel-43(sb41)* embryos have a tendency towards a symmetrical division.

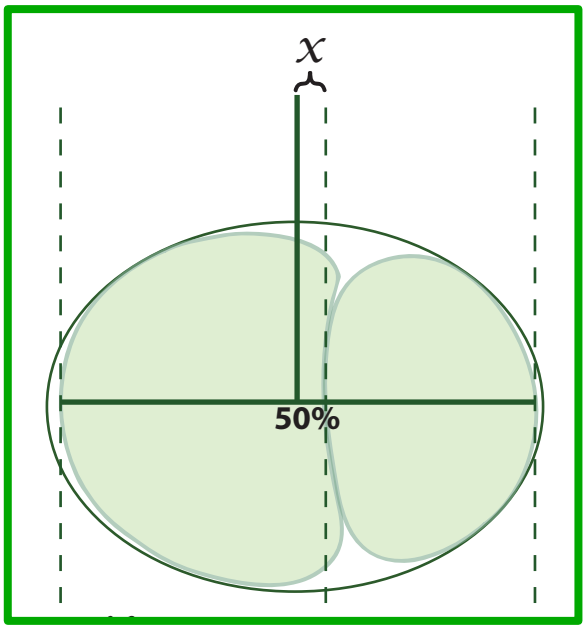

Figure 3-18. Measurements of embryo length can be used to determine the relative position of the cleavage furrow within the cell.

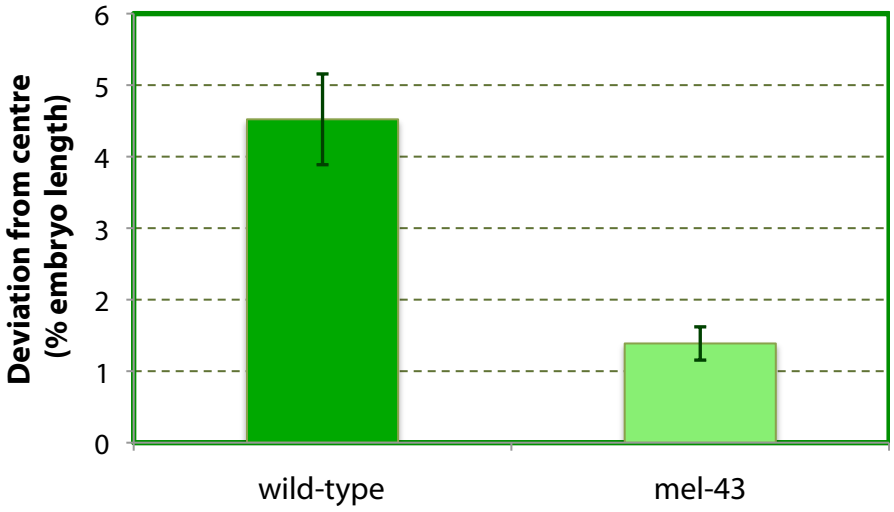

Figure 3-19. Cleavage furrow measurements of embryos. Cleavage Furrow position deviation from centre in *mel-43(sb41)* and wild-type embryos, as a measure of polarity establishment. Two cell *mel-43(sb41)* and N2 embryos were imaged using DIC microscopy. Measurements along the AP axis were taken and used to calculate the relative position of the cleavage furrow in the embryo, according to Figure 3-18. Standard error was calculated as a measure of significance (error bars). Measurements of ten embryos from each class were used to calculate the average deviation from centre as a percent of total embryo length.

3.9. Cyclin B1 degradation in *mel-43(sb41)* embryos

Eukaryotic cell cycle progression is regulated largely by the activity of cyclin-dependent kinase (CDK) family members. CDKs are activated when they are bound by cyclins, and this activity is also influenced by phosphorylation of the CDK itself. Temporal regulation of cyclin production and degradation drives the cell through the cell cycle. Targeted degradation of a cyclin, using ubiquitin complex machinery, inactivates the corresponding CDK. In *C. elegans* and higher eukaryotes, multiple CDKs partner with respective cyclin family members to drive the cell through both meiosis and mitosis.

In *C. elegans*, CDK1 binds the B-type cyclins, CYB-1 and CYB-3. Pre-formed Cyclin B-CDK1 complexes are kept inactive in the developing oocytes until the MSP signal is received to trigger the exit from meiotic arrest. Degradation of CYB-1 and CYB-3 is necessary for progression through meiosis. APC/C degrades cyclin B at the end of meiosis I, and the CUL-2/ZYG-11 complex degrades cyclin B at the end of meiosis II. Mutations in either of these pathways result in the persistence of B-type cyclins, which is detectable using a CYB-1 or CYB-3 fluorescent transgene. Because *mel-43(sb41)* embryos have an identified delay in meiosis II, one possibility is that they are defective in the CUL-2/ZYG-11 pathway. In order to determine whether *mel-43(sb41)* embryos are able to degrade CYB-1 (and presumably CYB-3), a CYB-1 fluorescent transgene was used to monitor degradation of CYB-1 over time. CYB-1

fluorescent levels are high in oocytes and then begin to decrease immediately following fertilization. To control for photobleaching, fluorescence in a multicellular embryo in the uterus was also assessed and the ratio was used to determine a relative fluorescence level. At least two embryos were used to determine cyclin B fluorescence levels in both *mel-43(sb41)* and wild-type over time (Figure 3-20). Standard error was calculated to attribute significance to the sample set.

In both wild-type and *mel-43(sb41)* embryos, CYB-1 levels begin to decrease similarly after spermatheca exit (time 0), when the ratio of fluorescence is approximately 2.35. At a time roughly corresponding to meiotic anaphase I (11-12 min), the fluorescence ratio declines to approximately 1.7. The fluorescence ratio continues to gradually decline reaching a value of approximately 1.5 at 35 minutes post-spermatheca exit

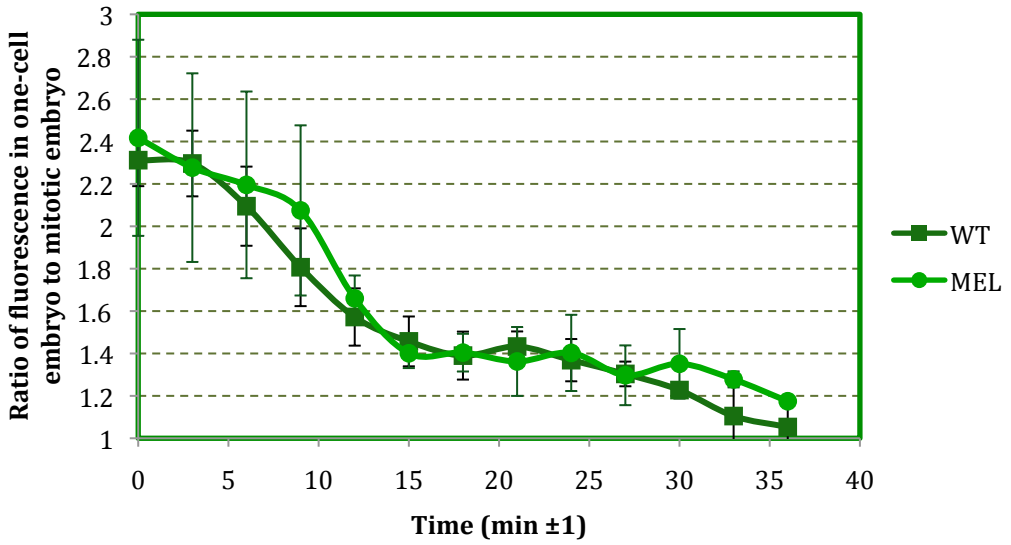

Figure 3-20. Cyclin B1 degradation in *mel-43(sb41)* and wild-type embryos, as measured by CYB-1::GFP fluorescence intensity over time. Time 0 refers to spermatheca exit. Integrated intensity using a set area was calculated for the embryo of interest as well as for a multicellular embryo already in the uterus, to account for photobleaching. The ratio of fluorescence intensity was calculated and plotted. A minimum of two embryos were used for each three minute timepoint per sample set. Times are accurate ±1 minute.

4. Discussion

4.1. Genomic location of *mel-43*

mel-43(sb41) was discovered in a screen for dominant, temperature-sensitive maternal-effect mutations. Preliminary characterization was performed on the mutation and three-factor mapping placed *mel-43* on chromosome IV, between *unc-24* and *fem-3*, a range of approximately 1 Mbp. Sequencing the entire region would be extremely laborious and time-intensive, and therefore was not an option to identify *mel-43*. Instead, an approach known as SNIP-SNP mapping was undertaken. Using a highly polymorphic Hawaiian isolate, CB4856, crossovers are able to provide informative details about the location of a mutation (reviewed in Materials and Methods). Prior to beginning SNIP-SNP mapping, it was necessary to encompass *mel-43(sb41)* by visible markers on both sides. Since *mel-43(sb41)* was already maintained in a strain containing *dpy-20* on the same chromosome, the ideal choice for the second marker, on the opposite side of *mel-43*, was *unc-24*. This would create the smallest marker-flanked region that is easily detectable on the plate as an Unc Dpy phenotype. Because *dpy-20* and *unc-24* create a new phenotype when present together, crossovers separating the markers to generate Unc non-Dpy and Dpy non-Unc worms are easily detectable.

A heterozygous strain containing *mel-43(sb41)* and *dpy-20* on one chromosome and *unc-24* on the other chromosome was generated. Heterozygotes were individually plated, allowed to self-fertilize, and F1 progeny were screened. Individual Unc progeny were plated at 25°C, with the reasoning that if a crossover had incorporated *unc-24* onto the original *mel-43(sb41) dpy-20* chromosome, Unc worms heterozygous for *mel-43(sb41)* (*i.e.*, *unc-24 mel-43(sb41) dpy-20/ unc-24*) would produce very few viable worms in a background of dead eggs. These worms could then be rescued by downshifting to 15°C, where 75% of the progeny are expected to hatch.

A pilot screen for Uncs that were Mel at 25°C resulted in an unexpectedly high proportion (over 5%) of Mel Uncs out of the total number of Uncs. This was surprising because *mel-43* was predicted to be 0.16 cM from *unc-24*, corresponding to a crossover frequency of 0.16%. The majority of these Uncs could not be maintained upon downshift to 15°C, possibly because of the age of the hermaphrodites. One Unc animal, however, was Mel at 25°C and 15°C, with a consistently low level of hatching (not 100% Mel), which allowed it to be recovered and maintained. This animal failed to give Unc Dpy progeny and was initially classified as an artifact of the screen. It was thought that perhaps the temperature-sensitive nature of the *mel-43(sb41)* allele was causing an unforeseen synthetic interaction with one of the visible markers. Therefore, the method of screening for Unc Mel Dpy recombinants was altered.

Using the same heterozygous strain, multiple individual hermaphrodites were allowed to self at 15°C. Single Uncs were plated at 15°C and plates that gave Unc Dpy progeny were selected for further analysis. From these plates, Unc Dpy animals were picked to separate plates and determined to be Mel or not by scoring for percent hatching. After looking at over 1400 individual Uncs, 29 were recovered that gave Unc Dpys (2%). This is consistent with the known genetic distance between *unc-24* and *dpy-20* (1.71 cM). However, none of these Unc Dpys were Mel. Purely by chance, one Unc recovered at 15°C was Mel but consistently failed to give Unc Dpy progeny, although hatching levels were sufficient to maintain the strain. These data, taken together with the previous Unc that was discovered to be Mel without the Dpy marker, led to a re-evaluation of the map position for *mel-43*. In two independent cases, Uncs were discovered that contained *mel-43(sb41)* but did not contain *dpy-20*. There are two possible explanations for these observations (Figure 4-1). Providing *mel-43* is in the previously published position, this result can best be explained by a double crossover linking *mel-43* to *unc-24* and excluding *dpy-20*. However, in order to generate an *unc-24 mel-43* homozygote, two such recombinant gametes would need to combine. This seems highly unlikely because one would expect a single crossover in the same region to be more common than a double crossover, and single crossovers were never detected. Furthermore evidence suggests that *C. elegans* chromosomes do not undergo multiple crossovers (reviewed by Hillers and Villeneuve, 2009). The second,

more likely possibility is that *mel-43* resides on the other side of *unc-24*, in which case a single crossover between *mel-43* and *unc-24* could exclude *dpy-20*. Again, because it was observed that these Uncs were completely Mel at 15°C, implying two copies of *mel-43(sb41)* are present, two of these gametes would have to combine to form a homozygous *unc-24 mel-43(sb41)* animal.

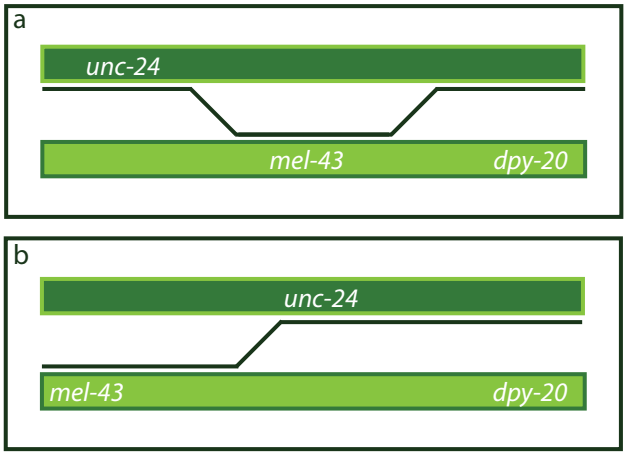

Figure 4-1. Two proposed possibilities to explain the origin of two independent Unc non-Dpy Mel progeny that were detected. a. A double crossover that places *unc-24* in cis with *mel-43(sb41)* while excluding *dpy-20* from the same chromosome. b. If *mel-43(sb41)* is not contained in the interval between *unc-24* and *dpy-20*, a single crossover would eliminate *dpy-20* while incorporating *unc-24*. The frequency of this event depends on the physical distance separating *unc-24* from *mel-43*.

The observation that Unc Mels never produced Unc Mel Dpy progeny was inconsistent with mapping data previously published for the *mel-43* gene. In order to distinguish between the two possibilities, namely to confirm that *mel-43* was further downstream than originally proposed, a second mapping experiment was designed.

A mapping heterozygote of the genotype *bli-6 unc-24/mel-43(sb41) dpy-20* was created and heterozygous hermaphrodites were allowed to self-fertilize (Figure 3-2). In order to gain a more complete representation of recombinant events, every F1 hermaphrodite (n=1421) was set up on an individual plate at 15°C and followed through to the F2 generation. This allowed the confident determination of each genotype with regards to the visible markers. Worms producing no viable progeny at 15°C were scored as Mel and assumed to be homozygous for *mel-43(sb41)*. Low levels of maternal-effect lethality, as with *mel-43(sb41)*/+ heterozygotes were not detectable at 15°C, therefore *mel-43(sb41)*/+ heterozygotes were not distinguishable from +/+. Unfortunately, the *bli-6* marker was not completely penetrant and was masked by the *dpy-20* allele. This effectively reduced the design of the experiment from a three-factor mapping screen to a two-factor mapping screen. Nonetheless, from this mapping strategy, it was confirmed that *mel-43* resides to the left of *unc-24*. Unfortunately, *mel-43* was also further downstream than the most distal marker, *bli-6*, so recombination data was only obtainable from one direction. A total of 79 recombinants were identified, and these could be separated into Dpy non-Mel and Mel non-Dpy progeny. Linkage analysis placed *mel-43* in the centre of chromosome IV, at 0.06 (Figure 3-2).

After generally mapping *mel-43* to the centre of the chromosome, two additional experiments were designed to further narrow the region containing *mel-43*. Using *dpy-13* as a central marker (as it lies at 0.0 on

chromosome IV), and either *unc-17 (to the left)* or *unc-5* (to the right) as secondary markers, two unique mapping strains were created (Figure 3-3). Because *mel-43* should reside exclusively either in the *unc-17 – dpy-13* interval or within the *dpy-13 – unc-5* interval, these mapping experiments were designed to conveniently narrow the region of interest. All 9 recombinants from the *dpy-13 unc-5* mapping heterozygote were non-Mel, whereas 10 out of 18 recombinants from the *unc-17 dpy-13* mapping heterozygote were Mel. Taken together, these data suggest that *mel-43* lies at -1.38, between *unc-17* and *dpy-13* (Figure 3-3).

The region between *unc-17* and *dpy-13* is approximately 620 kbp, and the previous mapping experiment examined a limited number of recombinants. In order to procure a more refined map position for *mel-43*, the experiment was scaled up and repeated. 69 *unc-17* non-*dpy-13* recombinants were tested for the presence of *mel-43(sb41)* at 25°C (Figure 3-3). From these recombinants, 15 were determined to lack *mel-43(sb41)*. Based solely on this round of mapping, *mel-43* was predicted to reside at -0.67 on chromosome IV (Figure 3-3). This experiment was also repeated for the interval between *dpy-13* and *unc-5*, however results were inconclusive, likely owing to the inconsistent phenotype of *unc-5(e53)*.

Although *mel-43* was originally mapped to 3.67 on chromosome IV (Mitenko *et al.,* 1997), this thesis provides evidence that this is not the case. Through a series of mapping experiments, *mel-43* has been confidently

mapped to a region between *unc-17* and *unc-5* on chromosome IV. Data from the most recent mapping experiment further suggests that *mel-43* resides at -0.67 on chromosome IV. In particular, *unc-5* was a difficult marker to use; and should be avoided in future mapping experiments because *unc-5* functions in DTC migration and the *unc-5(e53)* mutation causes misformed gonads that drastically decrease fecundity (Kruger *et al.,* 2004; personal observations). Further mapping work with different markers is therefore necessary to confidently narrow down and confirm the region. Once the prospective area has been narrowed down, *mel-43* can be identified by transformation rescue or genomic sequencing.

4.2. Candidate gene sequencing

4.2.1. C28C12.2

Prior to determining that *mel-43* had been incorrectly mapped, the published *mel-43*-containing region was scanned for candidate genes. One gene in particular, C28C12.2 - a predicted APC activator, was a very appealing candidate gene, given the APC's prominent regulatory role in the progression of meiosis, and the meiotic phenotype of *mel-43(sb41)*. Sequencing both the introns and exons of C28C12.2 did not highlight any differences between

wild-type worms and *mel-43(sb41)* homozygotes. C28C12.2 was therefore eliminated as a candidate locus for *mel-43*.

4.2.2. C33H5.4

After discovering that *mel-43* was actually further to the left of *unc-24*, but before knowing exactly where *mel-43* mapped to, the central region of chromosome IV was examined for candidates. One gene was particularly interesting: C33H5.4, also known as *klp-10*, is a non-functional kinesin that is thought to have arisen from a recent gene duplication of *klp-18*, a functional kinesin that organizes acentrosomal microtubules into a bipolar meiotic spindle (Segbert *et al.,* 2003). Although *mel-43(sb41)* embryos do not exhibit obvious defects in bipolar meiotic spindle assembly, it is conceivable that specific mutations could give rise to unique phenotypes. Importantly, few genes in this genetic interval have been implicated in meiotic processes (PhenoBank). In light of the fact that *mel-43(sb41)* was originally classified as a putative neomorph, with the corresponding null phenotype being wild-type (Mitenko *et al.,* 1997), a gene such as klp-10 that has redundant functions during meiosis seemed a reasonable candidate. Indeed, a deletion of *klp-10* is phenotypically wild-type; theoretically certain mutations could produce a neomorphic or novel function to this otherwise non-essential gene copy of *klp-18*. Revertants were also sequenced because it was reasoned that the revertants were putative null alleles and would likely be due to point mutations in the coding region – two revertants would likely have two

different point mutations, and therefore a mutation could be detected by comparison of revertant sequences. Sequencing of the entire gene in both wild-type, and proposed *mel-43(sb41)* revertants *sb41sb67* and *sb41sb69* recovered in the original reversion screen did not uncover any nucleotide differences. C33H5.4 was therefore eliminated as a candidate locus.

4.3. Genetic behaviour of *mel-43(sb41)*

The discovery that *mel-43* had been previously incorrectly mapped prompted a reevaluation of the genetic behaviour of *mel-43(sb41)*. For example, *mel-43(sb41)* was predicted to be a gain-of-function mutation, likely neomorphic. The phenotype of *mel-43(sb41) in trans* to a deficiency (*sb41/eDf18* or *sb41/eDf19*) or the putative loss-of-function revertants (*sb41/sb41sb67* or *sb41/sb69)*, was indistinguishable from the *mel-43(sb41)/+* heterozygote (Mitenko *et al.,* 1997). It was therefore concluded that changing the wild-type gene dose did not change the phenotype. This interpretation, combined with the assumption that the null phenotype was wild-type, deemed *mel-43(sb41)* neomorphic, likely interfering with some early embryonic function (Mitenko *et al.,* 1997).

Based on results presented in this thesis, the newly-proposed location of *mel-43* (IV:-0.67) is not covered by the deficiencies used in the original characterization, and therefore the data is invalid. In this case, an alternate

explanation for the recovery of revertants at high frequency can also be explained. The revertants recovered were likely due to recombination events that separated *mel-43(sb41)* from the visible markers thought to flank the mutation: because a crossover did not separate the two visible markers surrounding *mel-43(sb41)*, a reversion to wild-type was assumed to be due to a novel mutation. Therefore, these revertants likely contained wild-type copies of *mel-43*, and not null mutations.

In order to re-characterize the behaviour of the *sb41* allele, a deficiency strain was obtained from the *Caenorhabditis* Genetics Center. The deficiency *mDf9* spans the *dpy-13* locus, and therefore, could encompass the *mel-43* gene based on mapping data (Figure 3-2; Figure 3-3). The breakpoints for this deletion have been placed on the physical map. For example the left breakpoint is known to include gene *let-275* (IV: -0.19) but not gene *let-274* (IV: -1.75) and the right break point is known to include gene *let-284* (IV: 1.64) but not gene *spe-27* (IV: 2.45) (Wormbase). Therefore, if *mDf9* deletes the *mel-43* locus, it will provide valuable mapping information. Additionally, if the phenotype of *mel-43(sb41)/mDf9* is more severe than *mel-43(sb41)*/+, it would indicate that *mel-43(sb41)* is a loss-of-function mutation. When *mel-43(sb41)*/+ males were crossed to *mDf9*/nT1 hermaphrodites, the F1 progeny are expected to comprise the genotypes *mel-43/nT1*, *mel-43/mDf9*, *mDf9/nT1* and *+/nT1*. F1 progeny were allowed to self-fertilize prior to scoring for embryonic lethality. A cluster of F1 progeny gave embryonic lethality percentages similar

to that observed in *mel-43(sb41)* homozygotes at 15°C (Figure 3-5; Figure 3-6; Figure 3-7) This suggests that *mel-43(sb41)* is amorphic, or is a complete loss-of-function, as placing the mutation over the deficiency behaves the same way as the homozygote. However, it is important to remember that *mel-43(sb41)* is potentially more complicated – it is temperature-sensitive and semi-dominant. At 15°C, the temperature that this deficiency analysis was conducted at, the mutation behaves somewhat recessively, although there is an inherent amount of embryonic lethality (approximately 24.5%) attributed to the heterozygote. At 25°C, however, the mutation behaves dominantly, indicating an atypical amorphic allele. Dominant amorphic alleles often indicate haplo-insufficiency, where two copies of the gene are required to produce a normal phenotype. This is reasonable, as the deletion from the region, *mDf9*, appears to be slightly haplo-insufficient (based on inherent lethality in the heterozygote). One possibility that cannot be ruled out at this point, is that *mel-43(sb41)* may be antimorphic (*i.e.* dominant negative, where the mutant copy interferes with the remaining wild-type copy). This can be tested in the future by placing *mel-43(sb41)* over a gene duplication, such as *mDp4* in the region, and determining whether the phenotype is improved or worsened.

4.4. Cellular defects observed in *mel-43(sb41) embryos*

Over the course of this thesis, numerous *mel-43(sb41)* embryos were observed, and a range of phenotypes were observed. Many embryos appeared multi-nucleated, which was likely due to either chromosome segregation/polar body extrusion defects in meiosis or endo-reduplication in mitotic embryos with cytokinesis defects. In support of the latter, cellular blebs were observed *in utero* in meiotic embryos before being reabsorbed into the embryo, indicative of a defect in cytokinesis (Figure 3-10).

Perhaps the most startling cellular phenotypes were those that involved the microtubule cytoskeleton of the early embryo. Concentrated foci of microtubules were sometimes observed in the meiosis-mitosis cytoplasm of *mel-43* mutants. Although the reason for these structures is unknown, similar structures have been been previously observed in MAT (metaphase to anaphase transition-defective) mutants affecting meiosis I. It remains to be determined whether these foci were benign or if they contributed to the eventual embryonic death. Observations of the microtubules in vivo indicated that the transition from meiosis to mitosis was disrupted. In many embryos, the metaphase II spindle persisted at the presumptive anterior until it spontaneously disintegrated, or was torn apart by the robust mitotic centrosome-based microtubule arrays that formed at this time. More likely than not, these cellular phenotypes are owing to a delay in the completion of meiosis.

4.5. Timing of events in the single cell *mel-43(sb41)* embryo

During live imaging of *mel-43(sb41)* embryos, it appeared that *mel-43(sb41)* embryos were temporally delayed through the first cell cycle. In order to determine whether this delay was specific to a particular process or more general, embryos were carefully timed using developmental landmarks and *in vivo* imaging. The first division of *mel-43(sb41)* embryos was found to be significantly delayed in comparison to wild-type embryos. When the total elapsed time was broken down into meiosis I, meiosis II, and mitosis, the overall delay was attributed to delays in meiosis II only (Figure 3-12). Additionally, *mel-43(sb41)* embryos failed to extrude a second polar body, consistent with a defect in meiosis II (Figure 3-9; Figure 3-10). Conversely, meiosis I appeared normal regarding spindle morphology, dynamics, and timing (Figure 3-10; Figure 3-11; Figure 3-12). The onset of mitosis was somewhat variable, as it was difficult to determine when meiosis II was complete. Failure of meiosis II was determined to be the point when the meiotic spindle lost its structure and appeared to dissolve in the cytoplasm.

Progression through metaphase II is dependent on degradation of the B-type cyclins, CYB-1 and CYB-3. These end products are targeted for degradation by an E3 ligase complex containing the cullin protein CUL-2 and a substrate-recognition subunit, ZYG-11 (Figure 1-3; Liu *et al.,* 2004; Sonneville and Gönczy, 2004; Vasudevan *et al.,* 2007). In addition to regulating the metaphase II to anaphase II transition, CUL-2 participates in establishment of

A-P polarity, mitotic chromosome condensation and cytoplasmic organization. ZYG-11 interacts with CUL-2 via binding to the Elongin C (ELC-1), the complex adaptor protein (Figure 4-2). Additionally, a ubiquitin-like protein Elongin B and the RING finger box protein (RBX-1) are components of the complex (Liu *et al.,* 2004; Vasudevan *et al.,* 2007).

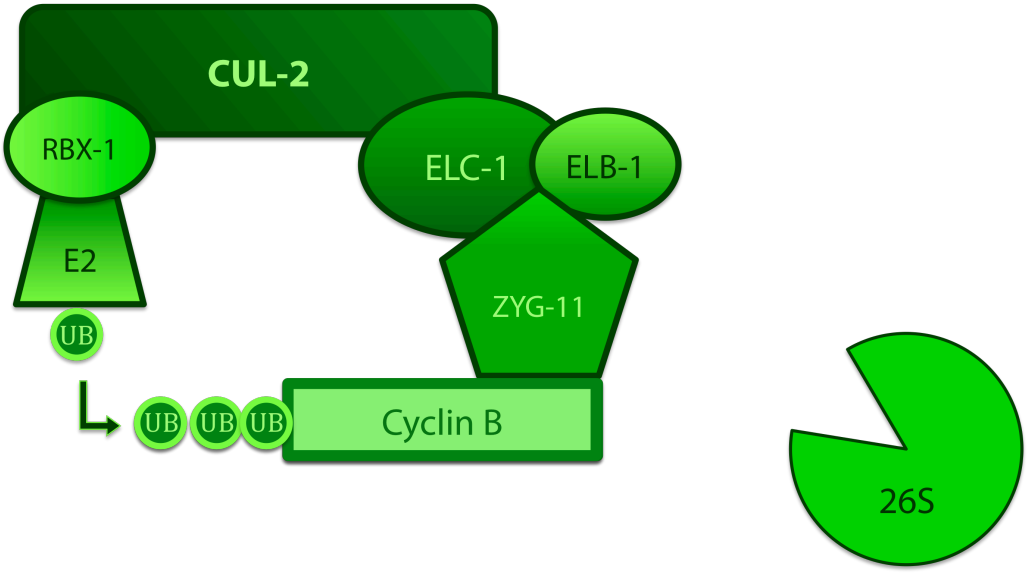

Figure 4-2. The CUL-2/ZYG-11 complex targets cyclin B for ubiquitin-mediated proteolysis by the 26S proteasome. Adapted from Kipreos, 2005.

Mutations in different components of this E3 complex result in a variety of phenotypes, however they all result in a metaphase II delay. CUL-2 mutants are most severe, with no discernable anaphase II prior to the appearance of the maternal pronucleus and extra karyomeres that form around unextruded meiosis II chromatin (Liu *et al.,* 2004). *cul-2* mutants usually arrest by the 24 cell stage. ZYG-11 mutants, on the other hand, eventually progress to anaphase II and segregate chromosomes, but fail to extrude a

polar body, thereby resulting in multiple nuclei (Liu *et al*., 2004). *zyg-11* mutants arrest at a later stage, with more cells than *cul-2* mutants (cite). *elc-1* mutants showed a range of phenotypes, from germ cell arrest to multiple nuclei, indicative of a polar body extrusion defect (Liu *et al.,* 2004). As a whole, it appears that there are different degrees of phenotypic severity depending on which complex component is affected. Because this is the only complex implicated specifically in the progression of meiosis II, it seems likely that *mel-43* is directly involved in the function or regulation of this complex, or is part of an as-of-yet unidentified pathway functioning downstream of the CUL-2/ZYG-11 pathway, but upstream of the microtubule rearrangements necessary to exit metaphase II.

4.6. Centrosomal maturation in *mel-43(sb41)* embryos

In some *mel-43(sb41)* embryos, centrosomes begin to nucleate microtubules prior to the completion of meiosis (personal observations). In wild-type embryos, the transition from meiosis to mitosis is carefully regulated, and centrosomes do not nucleate microtubules until meiosis is completed. Although the cell-cycle timing experiments indicated that the meiotic cell cycle is delayed, it was not clear whether the centrosome maturation cycle was also abnormal. For example, *mel-43(sb41)* mutants could cause inappropriate microtubule nucleation from centrosomes during

meiosis. Because the maturation of the centrosome involves numerous components acting collectively, it is conceivable that mis-regulation of microtubule nucleation could manifest as a change in the localization of centrosomal components, or regulators of microtubule outgrowth.

In order to examine the centrosomes of *mel-43(sb41)* embryos, three key centrosomally-located proteins were detected using fluorescently-labeled secondary antibodies. KLP-7, TAC-1, and γ-tubulin were analyzed in embryos from *mel-43(sb41)* homozygous parents. There was no obvious discrepancy between wild-type and *mel-43(sb41)* embryos with respect to KLP-7, TAC-1, or γ-tubulin at the centrosome. This suggested that these regulators of centrosomal microtubule outgrowth are not mislocalized, and probably do not directly cause premature microtubule outgrowth from the centrosomes.

4.7. Polarity establishment in *mel-43(sb41)* embryos

Initial DIC analysis showed that *mel-43(sb41)* two-cell embryos often divided synchronously (Mitenko *et al.,* 1997). This observation was confirmed in this thesis (Figure 3-16). In wild-type embryos the first division is asymmetric, producing a larger AB cell and a smaller P1 cell. In the second round of division, the AB cell divides before the P1 daughter cell. This asynchronous two-cell division and size asymmetry is a major consequence of proper polarity establishment in the single cell embryo (Budirahardja and

Gönczy, 2008; Reviewed in Rose and Kemphues, 1998). In order to examine whether or not polarity was properly established in *mel-43(sb41)* embryos, two approaches were used: direct measurement of the cleavage furrow placement within the cell, and direct observation of PAR protein localization.

One of the convenient cytological landmarks of "anterior" in the one-cell embryo is the position of the polar body. This is because, although the point of sperm entry specifies the posterior, the female meiotic divisions are usually completed at the opposite side of the cell. Polar bodies are easily detected with simple DIC microscopy. However, in some cases when meiosis fails, such as with *mel-43(sb41)* embryos, polar bodies are not reliably detected. Regardless of whether polar bodies are present or not, the first mitotic division should be asymmetric if polarity has been properly established. Therefore, using an unbiased approach to determine whether the *mel-43(sb41)* embryos have a defect in polarity, the relative amount of deviation from centre (regardless of direction) was used to determine the degree of asymmetry. Wild-type embryos had a larger deviation from the embryo centre than *mel-43(sb41)* embryos, suggesting that relative to wild-type, *mel-43(sb41)* embryos have a tendency to divide symmetrically in the first division (Figure 3-19). Standard error was calculated to attribute significance to the averaged sample sets. In *mel-43(sb41)* two-cell embryos, the cleavage furrow was offset by 1.4% embryo length, compared to a deviation of 4.5% embryo length in wild-type embryos (Figure 3-19). This suggests that *mel-43(sb41)* embryos do not divide

completely symmetrically, but the division is not as asymmetric as in wild-type embryos. It is unknown from this method whether the anterior cell is always slightly larger than the posterior cell, or if the slight average asymmetry reflects both anterior and posterior displacements from the centre point. Using DIC images as the source of measurements has a certain level of intrinsic error associated with it: if the embryo is not completely in line with the cover slip focal plane (*i.e.* on an angle), or if the eggshell causes distortion of the cells (*i.e.* perhaps measurements of cell volume or cortical surface area would improve upon the method), measurements that aren't entirely representative of the situation can be recorded. Regardless of this possible problem, the data confirms that there is a polarity defect in *mel-43(sb41)* embryos.

Using antibodies against PAR-1 and α-tubulin, and DAPI to detect DNA, immunofluorescence was performed on *mel-43(sb41)* embryos. In wild-type embryos, PAR-1 is found at the posterior cortex and the centrosomes (Figure 1-3). In *mel-43(sb41)* embryos, PAR-1 was often mislocalized and was not always present at the centrosomes (Figure 3-17). This is consistent with the observed loss of asymmetry in *mel-43(sb41)* one-cell embryos, and indicates that this mutation perturbs the cortical polarization process, in part, through the mislocalization of PAR-1. Interestingly, mutations in the CUL-2/ZYG-11 complex that perturb meiotic progression also disrupt polarity

establishment, presumably because of persistence of the meiotic spindle (Liu *et al.,* 2004).

4.8. Cyclin B1 degradation in *mel-43(sb41)* embryos

Degradation of cyclin B1 is required for the metaphase-to-anaphase transition in meiosis, and persistence of cyclin B has been identified as a marker of meiotic delays (Liu *et al.,* 2004; Sonneville and Gönczy, 2004). Using a fluorescent transgene, cyclin B levels in the embryo were detected over time to determine if *mel-43(sb41)* embryos are unable to degrade cyclin B. When compared to wildtype, there was no discernable difference in cyclin B levels over time in *mel-43(sb41)* homozygotes (Figure 3-20). This indicates that *mel-43(sb41)* is likely not defective in the CUL-2/ZYG-11 pathway, as one target is still degraded properly.

4.9. Future directions

4.9.1. Speculation on the function of *mel-43* in the cell

The question still remains as to what *mel-43* is doing in the cell. Although it has been shown that cyclin B1 degradation is unaffected in *mel-43(sb41)* embryos, there is still the possibility that *mel-43(sb41)* represents a substrate-specific mutation downstream of the CUL-2/ZYG-11 complex (Figure 4-3). An

additional possibility is that *mel-43(sb41)* acts downstream of the CUL-2/ZYG-11 pathway, but upstream of the microtubule arrangements that promote anaphase (Figure 4-3). During meiotic anaphase, there is an increase in midzone microtubules, functioning to force the chromosomes apart, while the spindle pole microtubules depolymerize (Albertson and Thomson, 1993). Because *mel-43(sb41)* mutants have a metaphase II spindle that maintains its structure for an extended period of time, it is possible that they are defective in the microtubule arrangements necessary for anaphase. Finally, *mel-43(sb41)* could be directly interfering with the physical release of sister chromatids at the level of sister chromatid cohesion (Figure 4-3). REC-8, a cohesin, must be cleaved from the centromeric regions on sister chromatids to allow for proper separation. This is regulated independently of the CUL-2/ZYG-11 pathway, and represents another potential pathway that *mel-43* could be functioning in.

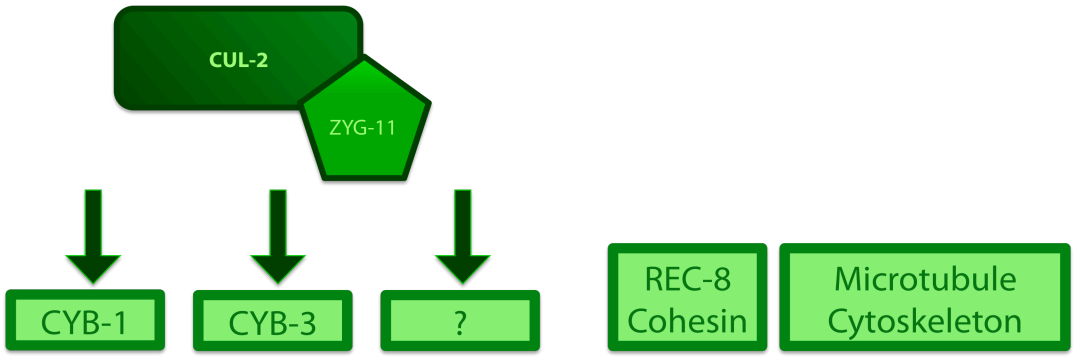

Figure 4-3. Potential pathways of involvement for *mel-43*. CUL-2/ZYG-11 is the primary regulator of meiosis II progression, and known downstream targets include cyclin B1 and cyclin B3, however it is possible that there are additional targets not yet identified. Although *mel-43(sb41)* embryos degrade CYB-1 normally, *mel-43(sb41)* could still be interfering with CYB-3 degradation or degradation of another substrate. Additionallly, *mel-43* could be required for cleavage of REC-8, allowing sister chromatids to separate, or for reorganization of the microtubule cytoskeleton to promote meiotic anaphase II.

4.9.2. Identification and cloning of *mel-43*

Although *mel-43* has been mapped to a relatively small genetic interval, further approaches need to be used in order to conclusively identify the *mel-43* locus and to subsequently clone it. One standard approach that has been very successful or identifiying genes in C. elegans is transformation resuce by microinjection (Mello *et al.,* 1991; Mello and Fire, 1995). If a duplication that spans the *mel-43* region is able to rescue the *mel-43(sb41)* phenotype at 15°C, this approach could be used to identify the *mel-43* gene. Therefore, *mel-*

43(sb41) should be placed over a duplication, *mDp4*, to see if it is able to ameliorate the phenotype.

Fosmids are bacterial vectors that can be used to propagate large pieces of genomic DNA. They are similar to cosmids except that they are more stable as they are maintained at a low copy number in the bacterial host (Geneservice). Overlapping fragments of DNA that span the entire *C. elegans* genome have been cloned into fosmid vectors and are available to the research community. After amplification and purification of the fosmid DNA, it is microinjected along with a co-transformation marker, *rol-6*, into the gonad of an L4 hermaphrodite. The two different plasmids are thought to undergo recombination reactions that create a large chimeric multi-copy array that may be incorporated into an oocyte nucleus during oogenesis. Positive Roller progeny (indicative of successful transformation) are then analyzed, as they are also expected to contain the extrachromosomal fosmid. Detection of *rol-6* is obscured in certain backgrounds, particularly in Unc and Dpy backgrounds. Therefore, the *mel-43*-containing strain HR592 is not ideal to perform fosmid injections (due to the dominant Unc in the *nT1[unc(n754dm) let]* balancer). Fortunately, the original *nT1* balancer lacks a dominant Unc and instead contains a recessive Vul (vulvaless) mutation that allows for easy identification of balancer homozygotes on a plate. To date, *mel-43(sb41)* has been re-balanced over the *nT1* translocation to produce a strain MAS87 that generates wild-type heterozygotes, Vul progeny, and Dpy-20 Mel progeny. Wild-type

worms will be injected and all Rol F1 progeny will be tested for stable transmission of the Rol-6 phenotype. Once a stable line is identified, the Dpy progeny from these worms could be tested for maternal-effect-lethality at 25°C. If a rescuing fosmid is identified, and more than one gene is present in the region, then subcloning of smaller fragments for injection would be used to identify the *mel-43* gene.

4.9.3. Non-complementation screen to identify new alleles

The sb41 allele is the only known mutation in the *mel-43* gene. The fact that it is dominant suggests that other mutations within the *mel-43* gene could result in a different phenotype. Therefore, in order to fully understand the function of this gene, it will be necessary to obtain more alleles. Results that indicate that the deletion *mDf9* fails to complement the *mel-43 (sb41)* mutation suggest that a standard non-complementation screen could be used to identify more loss-of-function alleles of *mel-43* (Figure 4-4). Because *mel-43(sb41)* is dominant, there are obvious difficulties associated with the design of a non-complementation screen; if *mel-43(sb41)* is amorphic, a second amorphic allele will fail to complement and essentially generate 100% maternal effect lethality at 15°C, making the new allele difficult, but not necessarily impossible, to recover. However, if a hypomorphic allele of *mel-43* were detected, an intermediate lethality would result for the heterozygote and the allele would be recovered with (relative) ease. Regardless, it is

advantageous to acquire multiple alleles of *mel-43*, as it makes further genetic techniques, including modifier screens, simpler.

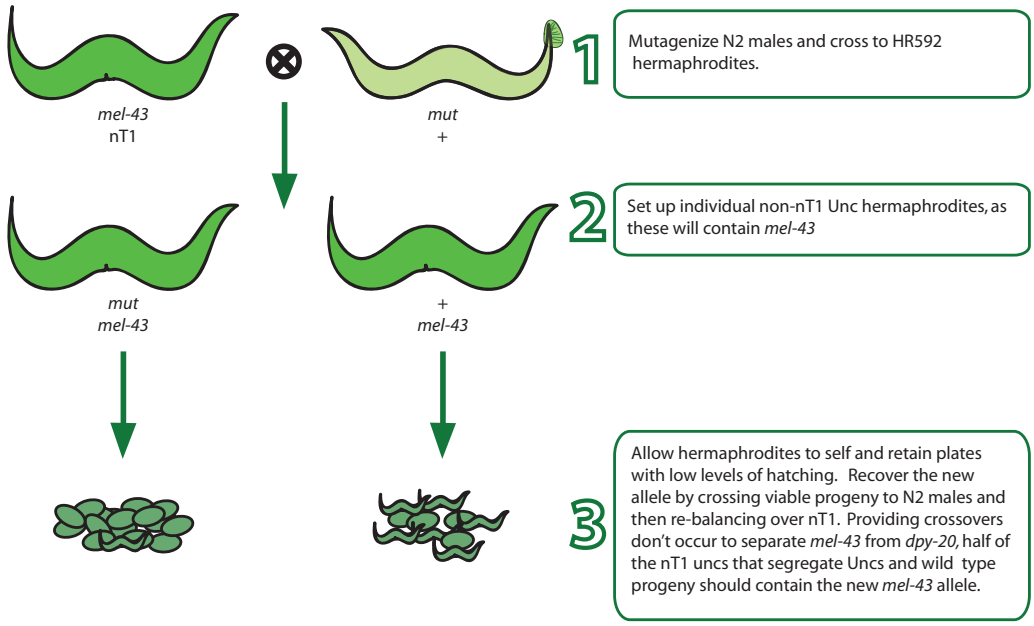

Figure 4-4. Non-complementation screen schematic for identifying new alleles of *mel-43*.

4.9.4. Modifier screen to identify pathway components

Work from this thesis suggests that *mel-43(sb41)* may be acting downstream of the CUL-2/ZYG-11 complex (as cyclin B is degraded normally) but upstream of the microtubule arrangements responsible for chromosome separation in anaphase II (as the metaphase spindle persists until dissolution and anaphase II doesn't occur). If *mel-43(sb41)* represents a new mechanism of regulation for meiosis II, it will be important to determine other pathway

components. This can be accomplished by performing a modifier screen. Essentially, mutagenesis is conducted in a *mel-43(sb41)*-sensitized background and mutations that suppress the phenotype (detectable by increased hatching in the *mel-43(sb41)* homozygote at 15°C) are further examined. Mutations that relieve the *mel-43(sb41)* embryonic lethality phenotype (suppressors) will provide valuable insight into the function that *mel-43* carries out in the cell. For example, if *mel-43* promotes cytoskeletal rearrangements in anaphase II and the sb41 allele is a loss-of-function mutation, the embryonic lethal phenotype could potentially be bypassed by a mutation that acts further downstream to constitutively activate the pathway. Prior to conducting a modifier screen, however, more alleles of *mel-43* should be generated as true bypass suppressors can be verified by testing their ability to suppress more than one allele of a gene

4.9.5. Candidate gene sequencing

One ongoing approach that should be continually pursued while *mel-43* is being identified by other means is sequencing of candidate genes. This thesis highlights the possibility that *mel-43* somehow ties into the pathway that is responsible for releasing the metaphase II to anaphase II inhibition, whether it be by releasing inhibition on a process or by promoting sister chromatid separation or cytoskeletal rearrangements (Figure 4-3).

Regulation of meiosis II is not clearly understood at this point. For example, the CUL-2/ZYG-11 complex has only recently been discovered, but its biological function is far from being completely understood. It is entirely conceivable that meiosis II-specific components exist that remain to be identified. Importantly, mutations in pathway component*s* that partake in both meiosis I and II could be categorized as having a meiosis I-specific phenotype, simply because that the early defect would obscure the later defect. Therefore, some previously characterized genes could be unintentionally overlooked when screening for candidate *mel-43* genes.

The dominant nature of the *sb41* allele leaves open the possibility that this phenotype might not be achievable through standard loss-of-function approaches, such as RNAi and candidate genes might not be apparent simply by screening through RNAi databases such as PhenoBank for a specific phenotype. In the future, approaches should be less restricted in order to not overlook valuable candidate genes.

5. Bibliography

Aceves, J., Erlij, D., Martinez-Maranon, R., 1970. The mechanism of the paralysing action of tetramisole on Ascaris somatic muscle. Br J Pharmacol. 38**,** 602-7.

Albertson, D. G., Thomson, J. N., 1993. Segregation of holocentric chromosomes at meiosis in the nematode, Caenorhabditis elegans. Chromosome Res. 1**,** 15-26.

Bellanger, J. M., Gonczy, P., 2003. TAC-1 and ZYG-9 form a complex that promotes microtubule assembly in C. elegans embryos. Curr Biol. 13**,** 1488-98.

Blackwell, T. K., Walker, A. K., 2008. OMA-gosh, where's that TAF? Cell. 135**,** 18-20.

Bowerman, B., Kurz, T., 2006. Degrade to create: developmental requirements for ubiquitin-mediated proteolysis during early C. elegans embryogenesis. Development. 133**,** 773-84.

Brenner, S., 1974. The genetics of Caenorhabditis elegans. Genetics. 77**,** 71-94.

Budirahardja, Y., Gonczy, P., 2008. PLK-1 asymmetry contributes to asynchronous cell division of C. elegans embryos. Development. 135**,** 1303-13.

Church, D. L., Guan, K. L., Lambie, E. J., 1995. Three genes of the MAP kinase cascade, mek-2, mpk-1/sur-1 and let-60 ras, are required for meiotic cell cycle progression in Caenorhabditis elegans. Development. 121**,** 2525-35.

Clandinin, T. R., Mains, P. E., 1993. Genetic studies of mei-1 gene activity during the transition from meiosis to mitosis in Caenorhabditis elegans. Genetics. 134**,** 199-210.

Clark-Maguire, S., Mains, P. E., 1994a. Localization of the mei-1 gene product of Caenorhaditis elegans, a meiotic-specific spindle component. J Cell Biol. 126**,** 199-209.

Clark-Maguire, S., Mains, P. E., 1994b. mei-1, a gene required for meiotic spindle formation in Caenorhabditis elegans, is a member of a family of ATPases. Genetics. 136**,** 533-46.

Cooke, J., Nowak, M. A., Boerlijst, M., Maynard-Smith, J., 1997. Evolutionary origins and maintenance of redundant gene expression during metazoan development. Trends Genet. 13**,** 360-4.

Cowan, C. R., Hyman, A. A., 2007. Acto-myosin reorganization and PAR polarity in C. elegans. Development. 134**,** 1035-43.

Cuenca, A. A., Schetter, A., Aceto, D., Kemphues, K., Seydoux, G., 2003. Polarization of the C. elegans zygote proceeds via distinct establishment and maintenance phases. Development. 130**,** 1255-65.

Davis, E. S., Wille, L., Chestnut, B. A., Sadler, P. L., Shakes, D. C., Golden, A., 2002. Multiple subunits of the Caenorhabditis elegans anaphase-promoting complex are required for chromosome segregation during meiosis I. Genetics. 160**,** 805-13.

Galli, M., van den Heuvel, S., 2008. Determination of the cleavage plane in early C. elegans embryos. Annu Rev Genet. 42**,** 389-411.

Golden, A., Sadler, P. L., Wallenfang, M. R., Schumacher, J. M., Hamill, D. R., Bates, G., Bowerman, B., Seydoux, G., Shakes, D. C., 2000. Metaphase to anaphase (mat) transition-defective mutants in Caenorhabditis elegans. J Cell Biol. 151**,** 1469-82.

Goldstein, B., Hird, S. N., 1996. Specification of the anteroposterior axis in Caenorhabditis elegans. Development. 122**,** 1467-74.

Goldstein, B., Hird, S. N., White, J. G., 1993. Cell polarity in early C. elegans development. Dev Suppl. 279-87.

Gomes, J. E., Encalada, S. E., Swan, K. A., Shelton, C. A., Carter, J. C., Bowerman, B., 2001. The maternal gene spn-4 encodes a predicted RRM protein required for mitotic spindle orientation and cell fate patterning in early C. elegans embryos. Development. 128**,** 4301-14.

Gonczy, P., Echeverri, C., Oegema, K., Coulson, A., Jones, S. J., Copley, R. R., Duperon, J., Oegema, J., Brehm, M., Cassin, E., Hannak, E., Kirkham, M., Pichler, S., Flohrs, K., Goessen, A., Leidel, S., Alleaume, A. M., Martin, C., Ozlu, N., Bork, P., Hyman, A. A., 2000. Functional genomic analysis of cell division in C. elegans using RNAi of genes on chromosome III. Nature. 408**,** 331-6.

Grishok, A., Sinskey, J. L., Sharp, P. A., 2005. Transcriptional silencing of a transgene by RNAi in the soma of C. elegans. Genes Dev. 19**,** 683-96.

Guo, S., Kemphues, K. J., 1996. Molecular genetics of asymmetric cleavage in the early Caenorhabditis elegans embryo. Curr Opin Genet Dev. 6**,** 408-15.

Hachet, V., Canard, C., Gonczy, P., 2007. Centrosomes promote timely mitotic entry in C. elegans embryos. Dev Cell. 12**,** 531-41.

Hang, J. S., Grant, B. D., Singson, A., 2008. Meiotic maturation: receptor trafficking is the key. Curr Biol. 18**,** R416-8.

Hao, Y., Boyd, L., Seydoux, G., 2006. Stabilization of cell polarity by the C. elegans RING protein PAR-2. Dev Cell. 10**,** 199-208.

Harris, J. E., Govindan, J. A., Yamamoto, I., Schwartz, J., Kaverina, I., Greenstein, D., 2006. Major sperm protein signaling promotes oocyte microtubule reorganization prior to fertilization in Caenorhabditis elegans. Dev Biol. 299**,** 105-21.

Hillers, K. J., Villeneuve, A. M., 2009. Analysis of meiotic recombination in Caenorhabditis elegans. Methods Mol Biol. 557**,** 77-97.

Hubbard, E. J., Greenstein, D., 2000. The Caenorhabditis elegans gonad: a test tube for cell and developmental biology. Dev Dyn. 218**,** 2-22.

Hubbard, E. J., Greenstein, D., 2005. Introduction to the germ line. WormBook. 1-4.

Johnston, W. L., Krizus, A., Dennis, J. W., 2006. The eggshell is required for meiotic fidelity, polar-body extrusion and polarization of the C. elegans embryo. BMC Biol. 4**,** 35.

Kadyk, L. C., Kimble, J., 1998. Genetic regulation of entry into meiosis in Caenorhabditis elegans. Development. 125**,** 1803-13.

Kemp, C. A., Kopish, K. R., Zipperlen, P., Ahringer, J., O'Connell, K. F., 2004. Centrosome maturation and duplication in C. elegans require the coiled-coil protein SPD-2. Dev Cell. 6**,** 511-23.

Kemphues, K. J., Wolf, N., Wood, W. B., Hirsh, D., 1986. Two loci required for cytoplasmic organization in early embryos of Caenorhabditis elegans. Dev Biol. 113**,** 449-60.

Kim, D. Y., Roy, R., 2006. Cell cycle regulators control centrosome elimination during oogenesis in Caenorhabditis elegans. J Cell Biol. 174**,** 751-7.

Kimble, J. E., White, J. G., 1981. On the control of germ cell development in Caenorhabditis elegans. Dev Biol. 81**,** 208-19.

Kipreos, E. T., 2005. Ubiquitin-mediated pathways in C. elegans. WormBook. 1-24.

Kruger, R. P., Lee, J., Li, W., Guan, K. L., 2004. Mapping netrin receptor binding reveals domains of Unc5 regulating its tyrosine phosphorylation. J Neurosci. 24**,** 10826-34.

Kuwabara, P. E., 2003. The multifaceted C. elegans major sperm protein: an ephrin signaling antagonist in oocyte maturation. Genes Dev. 17**,** 155-61.

Le Bot, N., Tsai, M. C., Andrews, R. K., Ahringer, J., 2003. TAC-1, a regulator of microtubule length in the C. elegans embryo. Curr Biol. 13**,** 1499-505.

Liu, J., Vasudevan, S., Kipreos, E. T., 2004. CUL-2 and ZYG-11 promote meiotic anaphase II and the proper placement of the anterior-posterior axis in C. elegans. Development. 131**,** 3513-25.

Matthews, L. R., Carter, P., Thierry-Mieg, D., Kemphues, K., 1998. ZYG-9, a Caenorhabditis elegans protein required for microtubule organization and function, is a component of meiotic and mitotic spindle poles. J Cell Biol. 141**,** 1159-68.

McCarter, J., Bartlett, B., Dang, T., Schedl, T., 1999. On the control of oocyte meiotic maturation and ovulation in Caenorhabditis elegans. Dev Biol. 205**,** 111-28.

Mello, C., Fire, A., 1995. DNA transformation. Methods Cell Biol. 48**,** 451-82.

Mello, C. C., Conte, D., Jr., 2004. Revealing the world of RNA interference. Nature. 431**,** 338-42.

Mello, C. C., Kramer, J. M., Stinchcomb, D., Ambros, V., 1991. Efficient gene transfer in C.elegans: extrachromosomal maintenance and integration of transforming sequences. EMBO J. 10**,** 3959-70.

Miller, M. A., Nguyen, V. Q., Lee, M. H., Kosinski, M., Schedl, T., Caprioli, R. M., Greenstein, D., 2001. A sperm cytoskeletal protein that signals oocyte meiotic maturation and ovulation. Science. 291**,** 2144-7.

Miller, M. A., Ruest, P. J., Kosinski, M., Hanks, S. K., Greenstein, D., 2003. An Eph receptor sperm-sensing control mechanism for oocyte meiotic maturation in Caenorhabditis elegans. Genes Dev. 17**,** 187-200.

Mitchison, T., Kirschner, M., 1984. Dynamic instability of microtubule growth. Nature. 312**,** 237-42.

Mitenko, N. L., Eisner, J. R., Swiston, J. R., Mains, P. E., 1997. A limited number of Caenorhabditis elegans genes are readily mutable to dominant, temperature-sensitive maternal-effect embryonic lethality. Genetics. 147**,** 1665-74.

Moritz, M., Braunfeld, M. B., Fung, J. C., Sedat, J. W., Alberts, B. M., Agard, D. A., 1995a. Three-dimensional structural characterization of centrosomes from early Drosophila embryos. J Cell Biol. 130**,** 1149-59.

Moritz, M., Braunfeld, M. B., Sedat, J. W., Alberts, B., Agard, D. A., 1995b. Microtubule nucleation by gamma-tubulin-containing rings in the centrosome. Nature. 378**,** 638-40.

Motegi, F., Seydoux, G., 2007. Revisiting the role of microtubules in C. elegans polarity. J Cell Biol. 179**,** 367-9.

Nance, J., 2005. PAR proteins and the establishment of cell polarity during C. elegans development. Bioessays. 27**,** 126-35.

Nebreda, A. R., Ferby, I., 2000. Regulation of the meiotic cell cycle in oocytes. Curr Opin Cell Biol. 12**,** 666-75.

O'Connell, K. F., Maxwell, K. N., White, J. G., 2000. The spd-2 gene is required for polarization of the anteroposterior axis and formation of the sperm asters in the Caenorhabditis elegans zygote. Dev Biol. 222**,** 55-70.

Oakley, B. R., 2000. An abundance of tubulins. Trends Cell Biol. 10**,** 537-42.

Ozlu, N., Srayko, M., Kinoshita, K., Habermann, B., O'Toole E, T., Muller-Reichert, T., Schmalz, N., Desai, A., Hyman, A. A., 2005. An essential function of the C. elegans ortholog of TPX2 is to localize activated aurora A kinase to mitotic spindles. Dev Cell. 9**,** 237-48.

Pasierbek, P., Jantsch, M., Melcher, M., Schleiffer, A., Schweizer, D., Loidl, J., 2001. A Caenorhabditis elegans cohesion protein with functions in meiotic chromosome pairing and disjunction. Genes Dev. 15**,** 1349-60.

Petronczki, M., Siomos, M. F., Nasmyth, K., 2003. Un menage a quatre: the molecular biology of chromosome segregation in meiosis. Cell. 112**,** 423-40.

PhenoBank, 2009. http://worm.mpi-cbg.de/phenobank2.

Pintard, L., Kurz, T., Glaser, S., Willis, J. H., Peter, M., Bowerman, B., 2003a. Neddylation and deneddylation of CUL-3 is required to target MEI-1/Katanin for degradation at the meiosis-to-mitosis transition in C. elegans. Curr Biol. 13**,** 911-21.

Pintard, L., Willis, J. H., Willems, A., Johnson, J. L., Srayko, M., Kurz, T., Glaser, S., Mains, P. E., Tyers, M., Bowerman, B., Peter, M., 2003b. The BTB protein MEL-26 is a substrate-specific adaptor of the CUL-3 ubiquitin-ligase. Nature. 425**,** 311-6.

Praitis, V., Casey, E., Collar, D., Austin, J., 2001. Creation of low-copy integrated transgenic lines in Caenorhabditis elegans. Genetics. 157**,** 1217-26.

Rose, L. S., Kemphues, K. J., 1998. Early patterning of the C. elegans embryo. Annu Rev Genet. 32**,** 521-45.

Samuel, A. D., Murthy, V. N., Hengartner, M. O., 2001. Calcium dynamics during fertilization in C. elegans. BMC Dev Biol. 1**,** 8.

Schlaitz, A. L., Srayko, M., Dammermann, A., Quintin, S., Wielsch, N., MacLeod, I., de Robillard, Q., Zinke, A., Yates, J. R., 3rd, Muller-Reichert, T., Shevchenko, A., Oegema, K., Hyman, A. A., 2007. The C. elegans RSA complex localizes protein phosphatase 2A to centrosomes and regulates mitotic spindle assembly. Cell. 128**,** 115-27.

Segbert, C., Barkus, R., Powers, J., Strome, S., Saxton, W. M., Bossinger, O., 2003. KLP-18, a Klp2 kinesin, is required for assembly of acentrosomal meiotic spindles in Caenorhabditis elegans. Mol Biol Cell. 14**,** 4458-69.

Seydoux, G., 2004. Surfing the actomyosin wave: polarization of the C. elegans zygote. Dev Cell. 7**,** 285-6.

Shakes, D. C., Sadler, P. L., Schumacher, J. M., Abdolrasulnia, M., Golden, A., 2003. Developmental defects observed in hypomorphic anaphase-promoting complex mutants are linked to cell cycle abnormalities. Development. 130**,** 1605-20.

Shirayama, M., Soto, M. C., Ishidate, T., Kim, S., Nakamura, K., Bei, Y., van den Heuvel, S., Mello, C. C., 2006. The Conserved Kinases CDK-1, GSK-3, KIN-19, and MBK-2 Promote OMA-1 Destruction to Regulate the Oocyte-to-Embryo Transition in C. elegans. Curr Biol. 16**,** 47-55.

Siomos, M. F., Badrinath, A., Pasierbek, P., Livingstone, D., White, J., Glotzer, M., Nasmyth, K., 2001. Separase is required for chromosome segregation during meiosis I in Caenorhabditis elegans. Curr Biol. 11**,** 1825-35.

Sonneville, R., Gonczy, P., 2004. Zyg-11 and cul-2 regulate progression through meiosis II and polarity establishment in C. elegans. Development. 131**,** 3527-43.

Spilker, A. C., Rabilotta, A., Zbinden, C., Labbe, J. C., Gotta, M., 2009. MAP Kinase Signaling Antagonizes PAR-1 Function During Polarization of the Early Caenorhabditis elegans Embryo. Genetics. 183**,** 965-77.

Srayko, M., Buster, D. W., Bazirgan, O. A., McNally, F. J., Mains, P. E., 2000. MEI-1/MEI-2 katanin-like microtubule severing activity is required for Caenorhabditis elegans meiosis. Genes Dev. 14**,** 1072-84.

Srayko, M., Kaya, A., Stamford, J., Hyman, A. A., 2005. Identification and characterization of factors required for microtubule growth and nucleation in the early C. elegans embryo. Dev Cell. 9**,** 223-36.

Srayko, M., O'Toole E, T., Hyman, A. A., Muller-Reichert, T., 2006. Katanin disrupts the microtubule lattice and increases polymer number in C. elegans meiosis. Curr Biol. 16**,** 1944-9.

Srayko, M., Quintin, S., Schwager, A., Hyman, A. A., 2003. Caenorhabditis elegans TAC-1 and ZYG-9 form a complex that is essential for long astral and spindle microtubules. Curr Biol. 13**,** 1506-11.

Stitzel, M. L., Pellettieri, J., Seydoux, G., 2006. The C. elegans DYRK Kinase MBK-2 Marks Oocyte Proteins for Degradation in Response to Meiotic Maturation. Curr Biol. 16**,** 56-62.

Strome, S., Powers, J., Dunn, M., Reese, K., Malone, C. J., White, J., Seydoux, G., Saxton, W., 2001. Spindle dynamics and the role of gamma-tubulin in early Caenorhabditis elegans embryos. Mol Biol Cell. 12**,** 1751-64.

Sundaram, M. V., 2006. RTK/Ras/MAPK signaling. WormBook. 1-19.

Takahashi, M., Iwasaki, H., Inoue, H., Takahashi, K., 2002. Reverse genetic analysis of the Caenorhabditis elegans 26S proteasome subunits by RNA interference. Biol Chem. 383**,** 1263-6.

Tsai, M. C., Ahringer, J., 2007. Microtubules are involved in anterior-posterior axis formation in C. elegans embryos. J Cell Biol. 179**,** 397-402.

Vale, R. D., 1991. Severing of stable microtubules by a mitotically activated protein in Xenopus egg extracts. Cell. 64**,** 827-39.

van den Heuvel, S., 2005. Cell-cycle regulation. WormBook. 1-16.

Vasudevan, S., Starostina, N. G., Kipreos, E. T., 2007. The Caenorhabditis elegans cell-cycle regulator ZYG-11 defines a conserved family of CUL-2 complex components. EMBO Rep. 8**,** 279-86.

Wallenfang, M. R., Seydoux, G., 2000. Polarization of the anterior-posterior axis of C. elegans is a microtubule-directed process. Nature. 408**,** 89-92.

Ward, S., Carrel, J. S., 1979. Fertilization and sperm competition in the nematode Caenorhabditis elegans. Dev Biol. 73**,** 304-21.

White, J., Strome, S., 1996. Cleavage plane specification in C. elegans: how to divide the spoils. Cell. 84**,** 195-8.

Wicks, S. R., Yeh, R. T., Gish, W. R., Waterston, R. H., Plasterk, R. H., 2001. Rapid gene mapping in Caenorhabditis elegans using a high density polymorphism map. Nat Genet. 28**,** 160-4.

Woollard, A., 2005. Gene duplications and genetic redundancy in C. elegans. WormBook. 1-6.

WormBase, http://www.wormbase.org WS207, October 19. 2009.

Wu, J. C., Rose, L. S., 2007. PAR-3 and PAR-1 inhibit LET-99 localization to generate a cortical band important for spindle positioning in Caenorhabditis elegans embryos. Mol Biol Cell. 18**,** 4470-82.

Yamamoto, I., Kosinski, M. E., Greenstein, D., 2006. Start me up: cell signaling and the journey from oocyte to embryo in C. elegans. Dev Dyn. 235**,** 571-85.

Yang, H. Y., McNally, K., McNally, F. J., 2003. MEI-1/katanin is required for translocation of the meiosis I spindle to the oocyte cortex in C elegans. Dev Biol. 260**,** 245-59.

Zetka, M., Rose, A., 1995. The genetics of meiosis in Caenorhabditis elegans. Trends Genet. 11**,** 27-31.